

NUMERICAL ANALYSIS AND SCIENTIFIC COMPUTING
PREPRINT SERIA

**Hybrid semi-Lagrangian finite
element-finite difference methods
for the Vlasov equation**

W. Guo J. Qiu

PREPRINT #21



DEPARTMENT OF MATHEMATICS
UNIVERSITY OF HOUSTON

OCTOBER 2013

Hybrid semi-Lagrangian finite element-finite difference methods for the Vlasov equation

Wei Guo¹ and Jing-Mei Qiu²

Abstract: In this paper, we propose a new conservative hybrid finite element-finite difference method for the Vlasov equation. The proposed methodology uses Strang splitting to decouple the nonlinear high dimensional Vlasov equation into two lower dimensional equations, which describe spatial advection and velocity acceleration/deceleration processes respectively. We then propose to use a semi-Lagrangian (SL) discontinuous Galerkin (DG) scheme (or Eulerian Runge-Kutta (RK) DG scheme with local time stepping) for spatial advection, and use a SL finite difference WENO for velocity acceleration/deceleration. Such hybrid method takes the advantage of DG scheme in its compactness and its ability in handling complicated spatial geometry; while takes the advantage of the WENO scheme in its robustness in resolving filamentation solution structures of the Vlasov equation. The proposed highly accurate methodology enjoys great computational efficiency, as it allows one to use relatively coarse phase space mesh due to the high order nature of the scheme. At the same time, the time step can be taken to be extra large in the SL framework. The quality of the proposed method is demonstrated via basic test problems, such as linear advection and rigid body rotation, and classical plasma problems, such as Landau damping and the two stream instability. Although we only tested 1D1V examples, the proposed method has the potential to be extended to problems with high spatial dimensions and complicated geometry. This constitutes our future research work.

Key Words: Vlasov equation, semi-Lagrangian method, hybrid method, discontinuous

¹Department of Mathematics, University of Houston, Houston, 77204-3008. E-mail: wguo126@math.uh.edu.

²Department of Mathematics, University of Houston, Houston, 77204-3008. E-mail: jingqiu@math.uh.edu. Research supported by National Science Foundation grant DMS-0914852 and the start up fund from University of Houston.

Galerkin method, WENO scheme, Landau damping, two stream instability.

1 Introduction

This paper will be focused on a high order Strang splitting conservative semi-Lagrangian (SL) approach for the Vlasov-Poisson (VP) simulations. Arising from collisionless plasma applications, the VP system,

$$\frac{\partial f}{\partial t} + \mathbf{v} \cdot \nabla_{\mathbf{x}} f + \mathbf{E}(\mathbf{x}, t) \cdot \nabla_{\mathbf{v}} f = 0, \quad (1.1)$$

and

$$\mathbf{E}(\mathbf{x}, t) = -\nabla_{\mathbf{x}}\phi(\mathbf{x}, t), \quad -\Delta_{\mathbf{x}}\phi(\mathbf{x}, t) = \rho(\mathbf{x}, t), \quad (1.2)$$

describes the temporal evolution of the particle distribution function in six dimensional phase space. $f(\mathbf{x}, \mathbf{v}, t)$ is probability distribution function which describes the probability of finding a particle with velocity \mathbf{v} at position \mathbf{x} at time t , \mathbf{E} is the electric field, and ϕ is the self-consistent electrostatic potential. The probability distribution function couples to the long range fields via the charge density, $\rho(t, x) = \int_{\mathbb{R}^3} f(x, v, t)dv - 1$, where we take the limit of uniformly distributed infinitely massive ions in the background. There are many challenges associated with the Vlasov simulations, the most important of which is probably the huge computational cost, due to the ‘curse of dimensionality’ (3D in physical space and 3D in velocity space). In this paper, we propose very high order numerical methods in order to resolve fine scale solution structures with relatively coarse numerical meshes.

Three different approaches in fusion simulations have been very popular, the Lagrangian (particle-in-cell (PIC)) [18, 27, 1, 19, 40, 25, 22], SL [38, 2, 3, 24, 39, 5, 33, 36, 37], and Eulerian approach [43, 41, 31, 42, 45, 21, 7]. Each approach has its own advantages and limits. For example, the PIC method is well known for its relatively low computational cost especially for high dimensional problems, compared with mesh-based methods. However, it suffers from statistical noise due to the initial sampling of macro-particles. The mesh-based

Eulerian approach suffers from ‘the curse of dimensionality’, a drawback compared with the PIC. On the other hand, Eulerian methods can be designed to be highly accurate, thus being able to resolve complicated solution structures in a more efficient manner by using a set of relatively coarse numerical mesh. One bottleneck of Eulerian methods, when applied to the VP system, is the *CFL* time step restriction. Compared with the Eulerian approach, the SL approach is also mesh based. Its distinctive feature lies in the fact that it allows for extra large time steps evolution, because information is being propagated along characteristics. On the other hand, the SL approach is more difficult to be implemented, as an accurate tracking of characteristics curve is highly nontrivial in nonlinear and truly multi-dimensional setting.

In kinetic simulations of plasma, a very popular approach is the Strang splitting SL method proposed by Cheng and Knorr [6]. The idea is that, rather than solving the truly multi-dimensional genuinely nonlinear VP system, Cheng and Knorr applied the Strang splitting to decouple the high dimensional nonlinear Vlasov equation (1.1) into a sequence of lower dimensional ‘linear’ equations. The advantage of performing such a splitting is that the decoupled lower dimensional advection equations have advection velocities depending only on the coordinates that are transverse to the direction of propagation. Therefore, as linear advection equations, they are much easier to be evolved numerically, especially in a SL setting.

Many advances in research have been made in developing mesh-based numerical algorithms for Vlasov simulations. A flux balanced semi-Lagrangian finite volume method was proposed in [14]; a flux-correct transport scheme was proposed in [4]; a high order cubic interpolated propagation method based on 1-D Hermite interpolation was proposed in [30]. Semi-Lagrangian scheme with high order cubic spline interpolation was proposed in [38]; later a positive and flux conservative finite volume semi-Lagrangian scheme with ENO reconstruction is proposed in [16]. A conservative finite volume and a non-conservative finite difference semi-Lagrangian scheme with WENO reconstruction is proposed in [5]. A con-

servative finite different semi-Lagrangian scheme with WENO reconstruction is proposed in [33]; later the algorithm is generalized to variable coefficient case [34, 35]. In the finite element discontinuous Galerkin framework, there are research work in Eulerian framework [21] and with positivity preserving limiters in semi-Lagrangian framework [37] and [36]. It is showed in [36] that the 1-D formulation of the algorithm is equivalent in [37] and [36] for constant coefficient case. In [36], a weak characteristic Galerkin approach is proposed for general variable coefficient case. 2-D implementation of the algorithm is different in [37] (modal) and [36] (nodal).

Despite the great convenience that the Strang splitting brought in for solving the Vlasov equation, there are several numerical challenges that need to be addressed for large scale realistic applications. For example, the computational domain in realistic simulation problems, e.g., tokamak, might be complicated. An unstructured mesh might be better suited for spatial discretization rather than the often used Cartesian meshes. Moreover, a well-known feature of the Vlasov solution is the development of filamentations, the resolution of which requires highly accurate and stable numerical methods. With these considerations, we propose a hybrid conservative SL method that uses finite element discontinuous Galerkin (DG) discretization in physical spaces, which is advantageous in its compactness and ability in handling complicated geometry and uses very high order SL finite difference weighted essentially non-oscillatory (WENO) discretization in velocity spaces, which is advantageous in its robustness, stability and ability in resolving complicated solution structures. When filamentation structures are under-resolved, numerical oscillations might be presented in the DG solutions. To reduce those oscillations, we apply WENO limiters [32], which are very robust for solutions with sharp gradients, yet can maintain high order spatial accuracy for smooth solutions. The proposed hybrid methodology is highly accurate and efficient, due to the very high spatial accuracy and the allowance of extra large time step evolution in the SL framework. Due to the dimensional splitting, the method suffers from the second order

splitting error in time. We plan to address this issue in our future research.

The rest of this paper is organized as follows. In Section 2, we review several existing numerical algorithms for advection problems, many of which will be used as basic ingredients in our proposed hybrid methodology. In Section 3, we describe the proposed methodology in great details. In this section, we frequently use 1D1V examples to illustrate the proposed idea. In Section 4, a collection of numerical examples are presented to demonstrate the performance of the proposed methods. The concluding remarks are given in Section 5.

2 High order mesh-based DG and WENO formulations

In this section, we discuss current state-of-the-art high order finite element and finite difference numerical techniques for hyperbolic problems. They serve as basic ingredients in the proposed methodology for the VP system in Section 3.

2.1 Eulerian approach: RK DG scheme.

The DG schemes [11, 10, 12, 9] are a class of high order numerical methods for solving a hyperbolic equation

$$f_t + \nabla \cdot \mathbf{g}(f) = 0. \quad (2.1)$$

For simplicity, we consider 1D domain $[a, b]$, which is partitioned as

$$\mathcal{D}_x : [a, b] = \cup_i I_i.$$

Let the solution and test function space be:

$$V_{\mathcal{D}_x}^k = \{u : u|_{I_i} \in P^k(I_i), \quad I_i \in \mathcal{D}_x\}. \quad (2.2)$$

The DG scheme approximates the weak form of hyperbolic equation (2.1) by finding $f_h \in V_{\mathcal{D}_x}^k$ such that for each cell I_i ,

$$\frac{d}{dt} \int_{I_i} f_h(t) \cdot u dx - \int_{I_i} g(f_h) \cdot u_x dx + \hat{g}_{i+\frac{1}{2}} \cdot u_{i+\frac{1}{2}}^- - \hat{g}_{i-\frac{1}{2}} \cdot u_{i-\frac{1}{2}}^+ = 0, \quad \forall u \in V_{\mathcal{D}_x}^k \quad (2.3)$$

where $\hat{g}_{i+\frac{1}{2}}$ is the numerical flux defined by an exact or approximate Riemann solver, e.g. Godunov flux, Lax-Friedrichs flux. Equation (2.3) is further discretized in time by a stable time integrator, such as high order strong stability preserving (SSP) RK method [20]. The most distinctive properties of DG schemes include their compactness, hp adaptivity and ability in handling complicated geometry. On the other hand, the numerical time step of the DG schemes is not only restricted by the CFL condition, but also by the linear stability property of the scheme, leading to roughly $|c|\frac{\Delta t}{\Delta x} \leq \frac{1}{2k+1}$ for a $(k+1)^{th}$ order scheme, where $|c|$ is the wave speed associated with a given problem.

It is known that spurious oscillations may appear in DG solutions, when there are shocks or sharp gradient structures involved. In order to suppress those numerical oscillations, nonlinear limiters, e.g. WENO limiter, are necessary. Nonlinear WENO limiting strategies have been developed based on WENO reconstruction in finite volume framework for structured and unstructured meshes [29, 26, 23]. The WENO limiting procedure consists of two steps: (1) Identification of troubled cells, using troubled cell indicator, e.g. the minmod-based TVB limiter [11, 10, 8, 12], in which the numerical solution involves large gradient; (2) In each trouble cell, replace the DG solution by a polynomial from WENO reconstruction. It is numerically shown in [32, 46] that the WENO limiters are very robust for solutions with sharp gradients, and they can achieve uniform high order accuracies for smooth solutions. For more technical details regarding WENO limiter, the readers are referred to [32].

2.2 Semi-Lagrangian approach: SL DG scheme

SL DG scheme differs from the RK DG scheme in its time evolution mechanism. Specially, characteristics are being tracked over time. The tracking of characteristic lines can be complicated for nonlinear and multi-dimensional problems. For simplicity, we only consider 1D linear equation (2.1) with $g = vf$, where v can be variable coefficient depending on x and t . The SL DG algorithm [36] is designed based on the semi-discrete DG scheme, see equation

(2.3). Specifically, we integrate equation (2.3) in time from $[t^n, t^{n+1}]$ and obtain,

$$\int_{I_i} f_h(t^{n+1}) \cdot u dx = \int_{I_i} f_h(t^n) \cdot u dx + \int_{t^n}^{t^{n+1}} \int_{I_i} v f_h \cdot u_x dx dt - \int_{t^n}^{t^{n+1}} (v \hat{f}_h \cdot u|_{x_{i+\frac{1}{2}}} - v \hat{f}_h \cdot u|_{x_{i-\frac{1}{2}}}) dt, \quad (2.4)$$

where the time integration of the flux function terms have to be evaluated in the SL fashion. To do that, we observe in Figure 2.1 that at a fixed spatial location at time level t^{n+1} , say $(x_{i-1/2}, t^{n+1})$, there exists a backward characteristic line (or curve when a is a function of x), with the foot located on time level t^n at $x_{i-1/2}^*$. We denote the region $\Omega_{i-1/2}$ to be the region bounded by the three points $(x_{i-1/2}, t^{n+1})$, $(x_{i-1/2}, t^n)$ and $(x_{i-1/2}^*, t^n)$. We apply the divergence theorem to the integral form of equation (2.1) over the region $\Omega_{i-1/2}$, and obtain

$$\int_{t^n}^{t^{n+1}} v \hat{f}_h(x_{i-1/2}, \tau) d\tau = \int_{x_{i-1/2}^*}^{x_{i-1/2}} f_h(\xi, t^n) d\xi, \quad (2.5)$$

which can be used to evaluate the time integration term on the r.h.s. of equation (2.4). For more implementation details, the readers are referred to [36]. The proposed SL DG scheme enjoys the advantages that (1) the scheme is of conservative form, where the flux function is evaluated exactly by equation (2.5); (2) it does not have the CFL /stability time step restriction as the Eulerian RK DG scheme [11], therefore allows for extra large time step evolution; (3) when compared with the finite difference WENO scheme, the proposed algorithm is more compact and allows for a non-uniform mesh for 1D problem. However, artificial oscillations may appear when filamentation structures developed in the Vlasov solutions are under-resolved. Nonlinear limiters, e.g. WENO limiter, are necessary to control spurious oscillations. The algorithm can be extended to multi-dimensional problems with Cartesian mesh by dimensional splitting. When the problem is linear, there is no splitting error involved as shown in Section 4. However, it is highly non-trivial to extend the proposed SL algorithm to unstructured grid in multi-dimension.

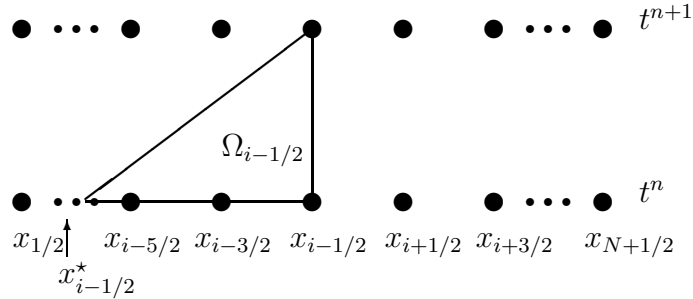


Figure 2.1: SL scheme approximates equation (3.9).

2.3 Semi-Lagrangian approach: SL finite difference WENO scheme

Another successful numerical method, in the class of finite difference schemes, for computational fluid dynamics (CFD) as well as kinetic simulations is the high order finite difference WENO scheme [26]. The SSP high order RK method can be used for time evolution. The most distinctive feature of finite difference WENO scheme is its ability in resolving complicated solution structures in a robust and stable way when compared with the DG scheme; as well as its ease and flexibility in multi-dimensional implementations by working with point values in a dimension-by-dimension fashion when compared with the finite volume method.

Similar to the SL DG scheme, instead of using SSP RK time integrator, one can use the SL evolution mechanism to evaluate the time integral of the flux functions. For more technical details, the readers are referred to [33, 34]. The advantage of doing so is the allowance of extra large numerical time steps that one can take. Either of the methods can be used for the VP applications [35]. However, the SL WENO scheme in [34] is more general in the sense that it can be used to deal with the variable coefficient advection problem, e.g. in solving the relativistic Vlasov equation.

In our Vlasov simulations, we adopt the SL WENO scheme in [33] for velocity accelera-

tion/deceleration. We consider equation (2.1) with constant wave speed as an example. The domain $[a, b]$ is uniformly discretized as:

$$a = x_0 < x_1 < \dots < x_{N-1} < x_N = b,$$

with $\Delta x = (b-a)/N$. Let $\Delta t = t^{n+1} - t^n$ and $\xi_0 = v \frac{\Delta t}{\Delta x}$. Without loss of generality, we assume $\xi_0 \in [0, \frac{1}{2}]$. When $\xi_0 \in [-\frac{1}{2}, 0]$, a similar but symmetric procedure can be applied. Otherwise, ξ_0 can be shifted to $[-\frac{1}{2}, \frac{1}{2}]$ via grid shifting. In the classical SL FD scheme, the solution is usually updated by using the fact that the solution is constant along characteristics [5], i.e.

$$f_i^{n+1} \doteq f(x_i, t^{n+1}) = f(x_i - v\Delta t),$$

where $f(x_i - v\Delta t)$ is usually reconstructed from neighboring point values by high order polynomial interpolation. Take a third order reconstruction for example, see Figure 2.2, we obtain

$$\begin{aligned} f_i^{n+1} &= f_i^n + \left(-\frac{1}{6}f_{i-2}^n + f_{i-1}^n - \frac{1}{2}f_i^n - \frac{1}{3}f_{i+1}^n\right)\xi_0 \\ &\quad + \left(\frac{1}{2}f_{i-1}^n - f_i^n + \frac{1}{2}f_{i+1}^n\right)\xi_0^2 \\ &\quad + \left(\frac{1}{6}f_{i-2}^n - \frac{1}{2}f_{i-1}^n + \frac{1}{2}f_i^n - \frac{1}{6}f_{i+1}^n\right)\xi_0^3, \end{aligned} \tag{2.6}$$

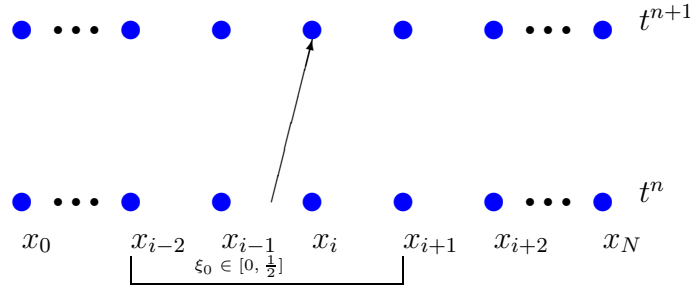


Figure 2.2: SL finite difference WENO reconstruction.

Based on the linear reconstruction, equation (2.6), a nonlinear WENO reconstruction can be introduced to suppress numerical oscillations known as Gibbs phenomenon when

the solution is under-resolved [5]. However, the mass conservation, which is a very important property for solving hyperbolic conservation laws, will be lost. To ensure the mass conservation, we re-write equation (2.6) in a flux difference form

$$f_i^{n+1} = f_i^n - \xi_0(\hat{f}_{i+1/2}^n - \hat{f}_{i-1/2}^n). \quad (2.7)$$

$\hat{f}_{i+1/2}^n$ is the numerical flux defined as

$$\hat{f}_{i+1/2}^n = (f_{i-1}^n, f_i^n, f_{i+1}^n) \cdot C_3^L \cdot (1, \xi_0, \xi_0^2)', \quad (2.8)$$

where

$$C_3^L = \begin{pmatrix} -\frac{1}{6} & 0 & \frac{1}{6} \\ \frac{5}{6} & \frac{1}{2} & -\frac{1}{3} \\ \frac{1}{3} & -\frac{1}{2} & \frac{1}{6} \end{pmatrix}.$$

Then, WENO reconstruction can be applied to the numerical flux $\hat{f}_{i+1/2}^n$. Such reconstruction algorithm can be generalized to higher order reconstructions, e.g. 5th, 7th and 9th. For more technical and implementation details, we refer the readers to [33].

3 Formulation of hybrid method

In this section, we will formulate the proposed hybrid method to solve the VP system. For Vlasov simulations, a very popular time stepping strategy is the Strang splitting [6]. There are many advantages associated with such splitting. For example, the nonlinearity of the VP system is being decoupled. As a result, the split equations can be independently evolved, for which a ‘best’ numerical method can be chosen for each of these independent evolutions. This idea of Strang splitting SL has been repeatedly applied in Vlasov simulations via different discretization strategy, e.g. the flux corrected transport [4], the flux balance method [14], the positive and flux conservative (PFC) method [16, 24], finite volume/difference WENO scheme [5, 33, 34, 35], discontinuous Galerkin (DG) scheme [36, 37], in the past decade. In

the proposed hybrid method we adopt the Strang splitting idea again. Especially, the six dimensional Vlasov equation (1.1) is splitted into two equations, for advection in space and velocity respectively,

$$\frac{\partial f}{\partial t} + \mathbf{v} \cdot \nabla_{\mathbf{x}} f = 0, \quad (3.9)$$

$$\frac{\partial f}{\partial t} + \mathbf{E}(\mathbf{x}, t) \cdot \nabla_{\mathbf{v}} f = 0. \quad (3.10)$$

The splitting of equation (1.1) can be designed to be second order accurate in time by advecting the equation (3.9) in spatial direction for a half time step, then evolving equation (3.10) in velocity direction for a full time step, followed by solving equation (3.9) for a second half time step. The two advection equations (3.9) and (3.10) are linear. They can be solved by independent numerical solvers, wisely chosen to be the most suitable ones for individual problems. For application problems such as tokamak, the spatial domain may have complicated geometry. Depending on the shape of spatial domain, we propose to apply the high dimensional (up to 3D) SL DG scheme or Eulerian DG scheme with local time stepping for equation (3.9) based on a structured rectangular or an unstructured triangular discretization of the spatial domain. On the other hand, the computational domain for velocity is simply a cuboid $\mathbf{v} \in [v_{1,min}, v_{1,max}] \times [v_{2,min}, v_{2,max}] \times [v_{3,min}, v_{3,max}]$ with zero boundary conditions. Because of this, we propose to apply the high order SL finite difference WENO scheme to evolve equation (3.10), which is very robust to resolve the filamentation solution structures in Vlasov simulations.

Below, we use an 1D1V example to illustrate the idea of the proposed hybrid scheme. The numerical mesh is based on a tensor product of the following discretization in x and v directions respectively,

$$\mathcal{D}_x : [a, b] = \cup_i I_i,$$

where I_i are non-overlapping intervals, not necessarily uniform, the union of which is the

interval $[a, b]$; and

$$\mathcal{D}_v : \quad c = v_{-N_v/2} < v_{-N_v/2+1} < \cdots < v_{-1} < v_0 < v_1 < \cdots < v_{N_v/2-1} < v_{N_v/2} = d,$$

where the distribution of grid points are uniform. The solution space for this 1D1V problem

$$V_{\mathcal{D}_{x,v}}^k = \{f(x, v = v_j)|_{I_i} := f_{i,j}(x) \in P^k, \quad i = 1, \dots, N_x, \quad j = -N_v/2, \dots, N_v/2\},$$

which is a piecewise polynomial defined on intervals of x , I_i , and at fix locations of v , v_j , $\forall i = 1, \dots, N_x$ and $j = -N_v/2, \dots, N_v/2$. The evolution procedure per time step Δt of the proposed splitting scheme for the VP system is described in the rest of this section. We remark that the time step Δt is not restricted by the *CFL*/stability constrain in our proposed framework.

3.1 Advection in spatial direction

We adopt SL or Eulerian DG scheme for advection in spatial direction, denoted as DG_x , discussed in details in Section 2.1 and 2.2. For each fixed grid point in velocity, say at v_j , we advect equation (3.9) for half a time step $\Delta t/2$.

- If SL DG approach is adopted, there is no *CFL*/stability time step restriction. Therefore, the time stepping for $\Delta t/2$ can be performed by calling $DG_x(\Delta t/2)$.
- If Eulerian DG, e.g. the RK DG, approach is applied, then there is time step restriction due to *CFL* and linear stability of the algorithm. We denote such the time step restriction as $\delta t(v_j)$, related to the wave propagation speed v_j . In this case, the time stepping for $\Delta t/2$ for the split 1-D linear equation can be performed by calling $DG_x^{loc}(\delta t(v_j))$ for several times (e.g. n times), until $\Delta t/2$ is reached. We write $DG_x(\Delta t/2) = (DG_x^{loc}(\delta t(v_j)))^n$. Such time stepping strategy maximizes the size of local time steps that can be applied in the RK DG scheme for (3.9) *per* v_j , hence optimizes the time stepping efficiency. Here, by ‘local’, we mean that the size of time

stepping can be chosen based on the wave propagation speed v 's. Much larger time step δt can be taken for smaller v 's. We remark that when a second or higher order SSP Runge-Kutta method is used, the proposed local time stepping strategy will not destroy the temporal accuracy, which is second order due to the splitting error.

The computational cost in computing one step of SSP RK3 DG would be proportional to $3(k+1)^2$; while that of SL DG would be proportional to $(k+1)^3$ when P^k polynomial space is used. However, compared with the SL DG approach, the RK DG approach will be more computationally expensive with the time step restriction due to linear stability and CFL condition ($CFL \leq \frac{1}{2k+1}$). Moreover, the temporal error of SL DG for 1-D problem would be smaller than that of SSP RK3 DG. On the other hand, extension of the RK DG algorithm to high dimensional \mathbf{x} is more flexible than that of SL DG. Unstructured triangular mesh depending on the shape of Ω is allowed in the RK DG framework. As we mention in Section 2.1, a nonlinear limiter is necessary to robustly resolve the filamentation solution structures of solution of the VP system. We will discuss this issue in Section 3.3.

3.2 Advection in velocity direction

A conservative high order SL finite difference WENO scheme, denoted as $SLWENO_v(\Delta t)$, discussed in Section 2.3, is applied to advect equation (3.10) for a time step Δt . As SL approach is applied, no time step restriction is involved in this step. Recall that the domain discretization of (x, v) is the tensor product of intervals (finite element discretization in x) and point values (finite difference discretization in v). In order to advect (3.10) by a finite difference scheme, we propose to apply one-to-one linear transformations from/to k^{th} degree polynomials $f_{i,j}(x)$ over I_i , to/from $(k+1)$ point values of the solution at Gaussian quadrature nodes on I_i at v_j , denoted as $\{f_{i,g_i;j}\}_{g_i=1}^{k+1}$. Here we propose to use Gaussian quadrature nodes as these nodes with the corresponding weights provide the most accurate weighted sum formula in evaluating the spatial integral term in DG formulation. Other

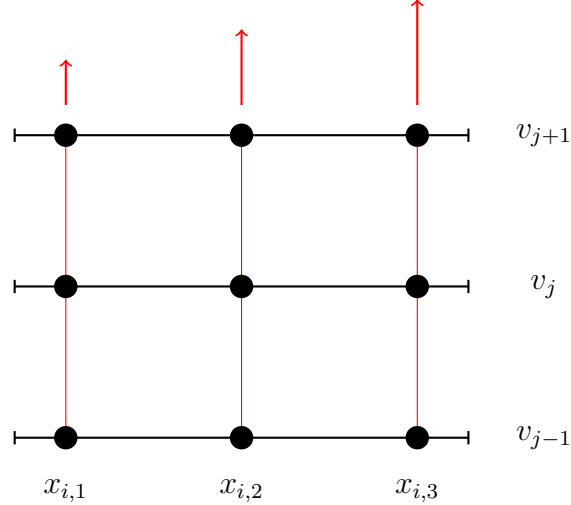


Figure 3.3: Advection in velocity direction by SL WENO scheme at Gaussian quadrature nodes. Piecewise polynomial space P^2 is used as an example.

choices of points, e.g. uniform, Gaussian-Radau, Gaussian-Lobatto points, can be used, but with lower order of accuracy in approximating the integral term in DG formulation. Below we illustrate the advection procedure (see Figure 3.3).

1. *From polynomials to point values.* For each spatial interval I_i , transform the k^{th} degree polynomial $f_{i,j}(x)$ to $k + 1$ Gaussian quadrature point values $\{f_{i,g_i;j}\}_{g_i=1}^{k+1}$ on I_i per grid point v_j .
2. *SL evolution.* Apply the SL FD WENO scheme, discussed in details in Section 3.3, on equation (3.10) for x_{i,g_i} , $\forall i = 1, \dots, N_x$ and $g_i = 1, \dots, k + 1$.
3. *From point values to polynomials.* For each spatial interval I_i , transform the $k + 1$ Gaussian quadrature point values $\{f_{i,g_i;j}\}_{g_i=1}^{k+1}$ back to a k^{th} degree polynomial $f_{i,j}(x)$, on I_i per grid point v_j .

Extension to high dimensional \mathbf{v} can be done by dimensional splitting without splitting error.

We remark that one has the flexibility to combine any order of SL/RK DG and SL WENO in the hybrid setting. In the simulations, we adopt the combination of P^1 with WENO3, P^2

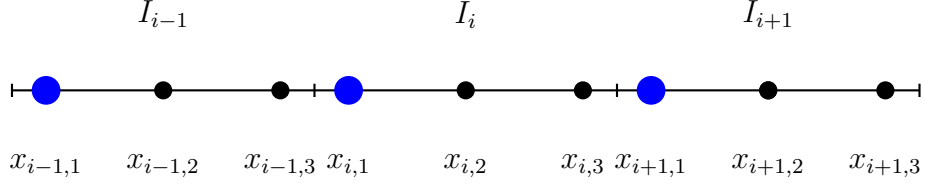


Figure 3.4: Evaluation of electric field by FFT at Gaussian quadrature nodes $\{x_{i,1}\}_{i=1}^{N_x}$. Piecewise polynomial space P^2 is used as an example.

with WENO5 and P^3 with WENO9 to better preserve the order of accuracy of DG scheme. We decide to use higher order WENO scheme than DG, as DG scheme has better resolution than WENO based on the same set of mesh. Specifically, DG scheme has $k+1$ degrees of freedom per cell compared with WENO which only has one point value.

In order to evolve the advection equation (3.10), the electric field needs to be computed. One can use a local discontinuous Galerkin scheme (LDG) to solve the Poisson equation (1.2). If the partition is uniform and periodic boundary condition is imposed, an alternative approach is to perform a fast Fourier transform (FFT). Firstly, we evaluate the charge density at all gaussian quadrature nodes. Then we group the points as $\{x_{i,g_l}\}_{i=1}^{N_x}$, $g_l = 1, 2 \dots k + 1$. Note that in each group, the nodes are evenly distributed. We can apply FFT in each group to get the electric field as showed in Figure 3.4. At each time step, FFT will be performed $k + 1$ times. Note that FFT is performed independently among different group. We remark that it is spectrally accurate to use FFT to solve the Poisson equation (1.2). Thus the error from solving the equation (1.2) is negligible compared with the error from solving Vlasov equation (1.1). We can also perform FFT on a set of uniform points without such grouping. However, it involves extra cost while little difference can be observed.

3.3 WENO limiter and algorithm flow chart

It is well known that filamentation solution structures can be developed in the VP system. So nonlinear limiters might be needed for DG scheme in spatial advection to control numerical

oscillations. We propose to apply the WENO limiter [32] before DG evolution as a pre-processing procedure. In our implementation presented in the next section, we use TVB limiter with problem dependent TVB constants to identify troubled cells. The flow chart of the algorithm is outlined below:

Algorithm: hybrid method for the Vlasov-Poisson system:

1. Evolve the solution in spatial directions by SL DG (or RK DG with local time stepping) for $\Delta t/2$ by calling $DG_x(\Delta t/2)$.
2. Solve E at all Gaussian points by FFT (or LDG) from the Poisson's equation.
3. Evolve the solution in velocity directions by SL FD WENO for Δt by calling $SLWENO_v(\Delta t)$.
4. Apply WENO limiter as a pre-processing procedure for DG evolution.
5. Evolve the solution as in step 1 for $\Delta t/2$.

Note that step 1 and step 4 can be merged as one time step in order to save cost.

Below we use the 2D rigid body rotation problem: $u_t - yu_x + xu_y = 0$ (Example 4.2) as an example to show the effectiveness of the proposed WENO limiter in pre-processing the DG solution. We consider the problem with computing domain $(x, y) \in [-3, 3] \times [-3, 3]$, initial condition $u(x, y, 0) = 0$ when $y < 0$ and $u(x, y, 0) = 1$ when $y \geq 0$ and periodic boundary condition. We evolve the equation by SL DG scheme P^3 in x-direction for $\Delta t/2$, then by SL FD WENO9 scheme in y-direction for Δt . 1D cuts of the numerical solution ($u(x, y=0)$) before and after WENO limiting procedure are shown in Figure 3.5. It can be observed that the total variation of the numerical solution is better controlled with the WENO limiter. We remark that the WENO limiter does not introduce much additional computational cost in our simulations presented in the next section, as the percentage of troubled cells where WENO limiters are applied is very small (less than 5%). In the simulation results, we also apply WENO limiters after DG evolutions in every time step to ensure that our numerical solution is oscillation-free. However, no significant difference is observed in the eye-ball norm

between the scheme with and without WENO after DG evolutions.

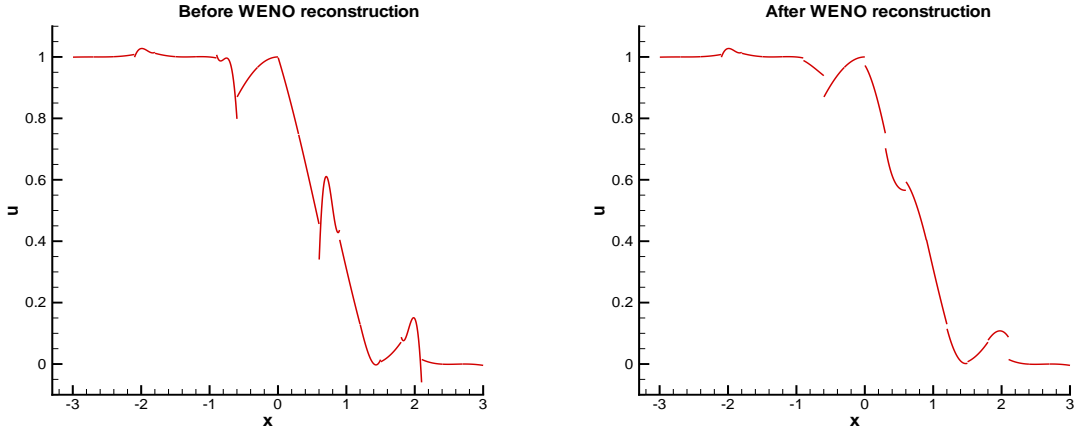


Figure 3.5: Solve $u_t + xu_y = 0$. Evolve the equation by SL WENO for one step. $N_x = N_y = 20$. $CFL = 2.2$. Before WENO reconstruction (left), after WENO reconstruction (right).

In the context of solving Vlasov equations, such WENO limiter would be useful when the initial data contains discontinuity. Even with smooth initial data, it is well-known that filamentation solution structures might be developed after some time. Such filamentation solution structures will be under-resolved by a given set of mesh. Numerical (rather than physical) oscillations might appear due to the Gibbs phenomenon. WENO limiter is adopted to control such oscillations for numerical stability. Notice that one can not hope for accuracy for under-resolve solution. Moreover, WENO limiter will not destroy the positivity, and one can apply a positivity preserving limiter proposed in [44] after WENO limiting procedure is used.

The proposed scheme cannot preserve the positivity, due to the fact that SL FD WENO scheme does not. A high order maximum principle preserving limiting procedure is proposed by Zhang and Shu in [44] for finite volume (FV) WENO scheme and DG scheme. Such limiting procedure cannot apply to FD WENO scheme directly. The reason is that FD

WENO reconstruction is based on a unknown function $g(x)$ whose sliding average is $f(x)$:

$$f(x) = \frac{1}{h} \int_{x-\frac{h}{2}}^{x+\frac{h}{2}} g(\xi) d\xi. \quad (3.11)$$

g function has a larger upper bound and smaller lower bound than f . In other words, $f \geq 0$ does not imply $g \geq 0$. Enforcing $g \geq 0$ will destroy the high order accuracy of reconstruction.

Finally, we remark that the proposed hybrid method is mass conservative, since the RK DG, SL DG and SL FD WENO schemes are all mass conservative. The mass conservation of DG scheme can be checked by choosing the test function $u = 1$ in the DG weak formulation (2.3). The mass conservation of SL FD WENO scheme is due to the fact that the equation (2.7) is in flux difference form. Readers are referred to [33, 36] for detail analysis.

Proposition 3.1 The proposed hybrid method conserves the total mass with periodic boundary condition.

Proof: It is sufficient to prove that the hybrid method is mass conservative without WENO limiter. The WENO limiter preserves the cell average, therefore the overall mass. We denote $\bar{f}_{i,j}^n$ as the cell average of the numerical solution $f_{i,j}$ over interval I_i at velocity v_j at time t^n . Denote $f_{i,j}^{n,(1)}$ as the numerical solution after advection of Step 1. Denote $f_{i,j}^{n,(2)}$ as the

numerical solution after advection in Step 3.

$$\begin{aligned}
\sum_j \sum_i \bar{f}_{i,j}^{n+1} \Delta x_i \Delta v &\stackrel{\text{Step 5}}{=} \sum_j \sum_i \bar{f}_{i,j}^{n,(2)} \Delta x_i \Delta v && \text{(mass conservation of DG)} \\
&= \sum_j \sum_i \Delta x_i \sum_{g_i} f_{i,g_i;j}^{n,(2)} w_{g_i} \Delta v \\
&= \sum_i \Delta x_i \sum_{g_i} w_{g_i} \sum_j f_{i,g_i;j}^{n,(2)} \Delta v \\
&\stackrel{\text{Step 3}}{=} \sum_i \Delta x_i \sum_{g_i} w_{g_i} \sum_j f_{i,g_i;j}^{n,(1)} \Delta v && \text{(mass conservation of SL WENO)} \\
&= \sum_j \sum_i \Delta x_i \sum_{g_i} f_{i,g_i;j}^{n,(1)} w_{g_i} \Delta v \\
&= \sum_j \sum_i \bar{f}_{i,j}^{n,(1)} \Delta x_i \Delta v \\
&\stackrel{\text{Step 1}}{=} \sum_j \sum_i \bar{f}_{i,j}^n \Delta x_i \Delta v && \text{(mass conservation of DG) } \blacksquare
\end{aligned}$$

4 Numerical results

In this section, several numerical examples are presented to illustrate high order accuracy and reliability of the proposed hybrid method. We test linear advection and rigid body rotation problems in Section 4.1, and the VP system in Section 4.2. In the numerical experiments below, two types of hybrid methods are considered. Especially, we first perform the dimensional splitting, then (1) SL DG or (2) RK DG with local time stepping for advection in x-direction are coupled with the SL FD WENO for advection in y- or v- direction.

4.1 Two-dimensional test examples

Example 4.1. Consider a two-dimensional linear advection equation:

$$u_t + u_x + u_y = 0 \tag{4.1}$$

with initial condition $u_0(x, y) = \sin(x + y)$ and periodic boundary condition. The errors and numerical orders of accuracy of the proposed hybrid methods are shown in Table 4.1 for

SL DG combined with SL WENO and in Table 4.2 for RK DG combined with SL WENO. Since the x-shifting and y-shifting operator commute, there is no splitting error in time and the spatial error dominates. We remark that we use higher order WENO reconstruction in y-direction than the order of DG in x-direction. Such choice of combination makes the DG error be the dominant error. Expected orders of accuracy from DG scheme are observed in Table 4.1 and 4.2. Comparable numerical results are observed for SL and RK DG scheme.

Table 4.1: Linear advection. Hybrid method with SL DG and SL WENO. L^2 errors and numerical orders of accuracy on uniform meshes with $N_x \times N_y$ cells. TVB constant $M=1.0$. $CFL=2.2$. $T=10$.

	$P^1 + WENO3$		$P^2 + WENO5$		$P^3 + WENO9$	
mesh	L^2 error	order	L^2 error	order	L^2 error	order
40×40	5.58E-2	–	8.67E-5	–	6.63E-7	–
80×80	1.87E-2	1.57	1.04E-5	3.06	4.05E-8	4.04
120×120	9.03E-3	1.79	3.12E-6	2.97	8.73E-9	3.78
160×160	4.96E-3	2.08	1.41E-6	2.75	2.77E-9	3.99
200×200	2.88E-3	2.44	6.81E-7	3.27	1.17E-9	3.87

Table 4.2: Linear advection. Hybrid method with RK DG and SL WENO. L^2 errors and numerical orders of accuracy on uniform meshes with $N_x \times N_y$ cells. TVB constant $M=1.0$. $CFL=2.2$. $T=10$.

	$P^1 + WENO3$		$P^2 + WENO5$		$P^3 + WENO9$	
mesh	L^2 error	order	L^2 error	order	L^2 error	order
40×40	5.04E-2	–	1.34E-4	–	8.10E-7	–
80×80	1.48E-2	1.77	1.36E-5	3.30	5.07E-8	4.00
120×120	7.03E-3	1.83	3.89E-6	3.09	1.00E-8	4.00
160×160	3.95E-3	2.00	1.62E-6	3.04	3.17E-9	4.00
200×200	2.40E-3	2.24	8.25E-7	3.03	1.30E-9	4.00

Example 4.2. Consider the rigid body rotation problem:

$$u_t - yu_x + xu_y = 0, \quad (x, y) \in [-2\pi, 2\pi] \times [-2\pi, 2\pi]. \quad (4.2)$$

Table 4.3: Rigid body rotation. Hybrid method with SL DG and SL WENO. L^2 errors and numerical orders of accuracy on uniform meshes with $N_x \times N_y$ cells. TVB constant $M=1.0$. $CFL=0.3$. $T=\pi/2$.

	$P^1 + WENO3$		$P^2 + WENO5$		$P^3 + WENO9$	
mesh	L^2 error	order	L^2 error	order	L^2 error	order
10×30	2.57E-01	–	6.09E-02	–	5.36E-03	–
20×60	7.33E-02	1.81	6.63E-03	3.20	3.41E-04	3.97
30×90	3.28E-02	1.98	1.90E-03	3.09	6.44E-05	4.11
40×120	1.88E-02	1.94	7.92E-04	3.03	2.01E-05	4.04
50×150	1.24E-02	1.88	4.15E-04	2.89	8.35E-06	3.95

We first consider a smooth initial condition

$$u(x, y, 0) = \begin{cases} \cos^6(\frac{r}{2}) & r < \pi, \\ 0 & \text{otherwise,} \end{cases} \quad (4.3)$$

where $r = \sqrt{0.8(x-1)^2 + 1.2y^2}$. This is to test order of convergence of the hybrid schemes. We report the L^2 error and the order of accuracy for two hybrid methods: SL DG combined with SL WENO in Table 4.3 and Table 4.4, RK DG combined with SL WENO in Table 4.5 and Table 4.6 for $CFL = 0.3$ and $CFL = 6.2$ respectively. The spatial error is observed to be the dominant error when $CFL = 0.3$, see Table 4.3 and 4.5. The second order splitting error in time becomes the dominant error when relatively large CFL is used, see Table 4.4 and 4.6. We remark that there is a certain range of CFL above which the splitting error in time is the dominant error. Such range is problem and scheme dependent. Improving such splitting error constitutes our future research work. Note that we set $3N_x = N_y$ in order to obtain a clean order of convergence from DG.

We then consider the initial condition that includes a slotted disk, a cone as well as a smooth hump, similar to the one in [28] to test our scheme's ability in resolving complicated structures. In Figure 4.1 we plot the initial condition in mesh and contour. We plot the numerical solution at $T = 12\pi$ in Figure 4.2, which is the return of the initial state after six full revolutions. Non-oscillatory numerical capturing of discontinuities is observed. It

Table 4.4: Rigid body rotation. Hybrid method with SL DG and SL WENO. L^2 errors and numerical orders of accuracy on uniform meshes with $N_x \times N_y$ cells. TVB constant $M=1.0$. $CFL=6.2$. $T=\pi/2$

	$P^1 + WENO3$		$P^2 + WENO5$		$P^3 + WENO9$	
mesh	L^2 error	order	L^2 error	order	L^2 error	order
10×30	1.87E-01	–	5.37E-02	–	2.67E-02	–
20×60	5.57E-02	1.75	8.03E-03	2.74	6.46E-03	2.05
30×90	2.53E-02	1.94	3.12E-03	2.33	2.87E-03	2.01
40×120	1.46E-02	1.92	1.66E-03	2.20	1.61E-03	2.00
50×150	9.71E-03	1.82	1.03E-03	2.12	1.03E-03	2.00

Table 4.5: Rigid body rotation. Hybrid method with RK DG and SL WENO. L^2 errors and numerical orders of accuracy on uniform meshes with $N_x \times N_y$ cells. TVB constant $M=1.0$. $CFL = 0.3$. $T=\pi/2$.

	$P^1 + WENO3$		$P^2 + WENO5$		$P^3 + WENO9$	
mesh	L^2 error	order	L^2 error	order	L^2 error	order
10×30	2.71E-01	–	6.75E-02	–	6.85E-03	–
20×60	7.87E-02	1.78	7.38E-03	3.19	6.15E-04	3.48
30×90	3.53E-02	1.98	2.14E-03	3.06	1.21E-04	4.01
40×120	2.00E-02	1.98	8.96E-04	3.02	3.83E-05	4.00
50×150	1.29E-02	1.95	4.66E-04	2.93	1.59E-05	3.94

Table 4.6: Rigid body rotation. Hybrid method with RK DG and SL WENO. L^2 errors and numerical orders of accuracy on uniform meshes with $N_x \times N_y$ cells. TVB constant $M=1.0$. $CFL = 6.2$. $T=\pi/2$

	$P^1 + WENO3$		$P^2 + WENO5$		$P^3 + WENO9$	
mesh	L^2 error	order	L^2 error	order	L^2 error	order
10×30	2.34E-01	–	6.57E-02	–	2.49E-02	–
20×60	6.92E-02	1.76	9.04E-03	2.86	6.15E-03	2.01
30×90	3.10E-02	1.98	3.36E-03	2.44	2.72E-03	2.01
40×120	1.76E-02	1.96	1.74E-03	2.29	1.53E-03	2.00
50×150	1.14E-02	1.95	1.06E-03	2.20	9.77E-04	2.00

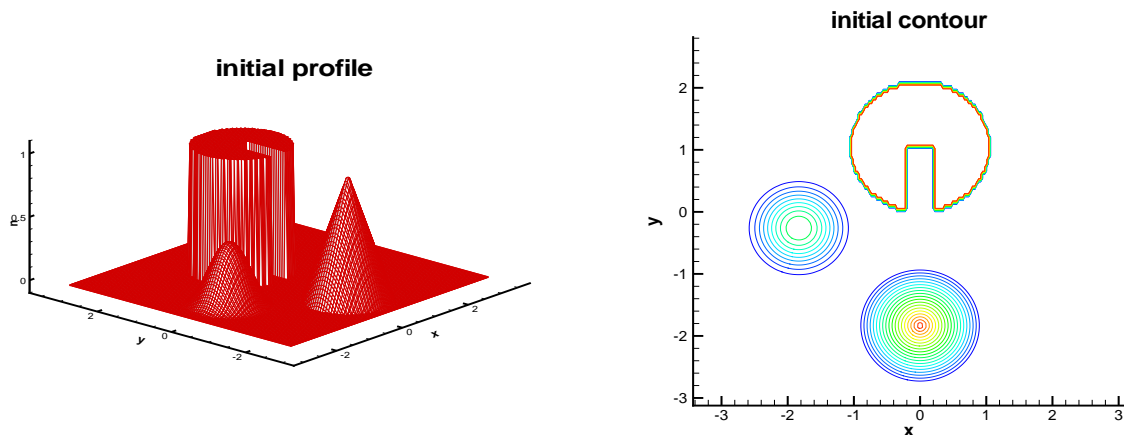


Figure 4.1: Initial condition. Profile (left) and contour (right).

is clear that higher order methods resolve the solution better. As the performance of the hybrid scheme using RK DG in x-direction is very similar to those in Figure 4.2, we omit them to save space.

4.2 The Vlasov-Poisson system

In this subsection, we further examine the performance of the proposed hybrid methods when applied to the VP systems. Periodic boundary condition is imposed in x-direction, while zero boundary condition is imposed in v-direction. We only present the numerical results of the hybrid method with SL DG in x-direction and SL WENO in v-direction, as the performance of the scheme using RK DG for spatial advection is very similar. In realistic high dimensional problems with complicated spatial domains, RK DG will offer more flexibility than SL DG. We recall several norms in the VP system below, which should remain constant in time.

1. L^p norm $1 \leq p < \infty$:

$$\|f\|_p = \left(\int_v \int_x |f(x, v, t)|^p dx dv \right)^{\frac{1}{p}}. \quad (4.4)$$

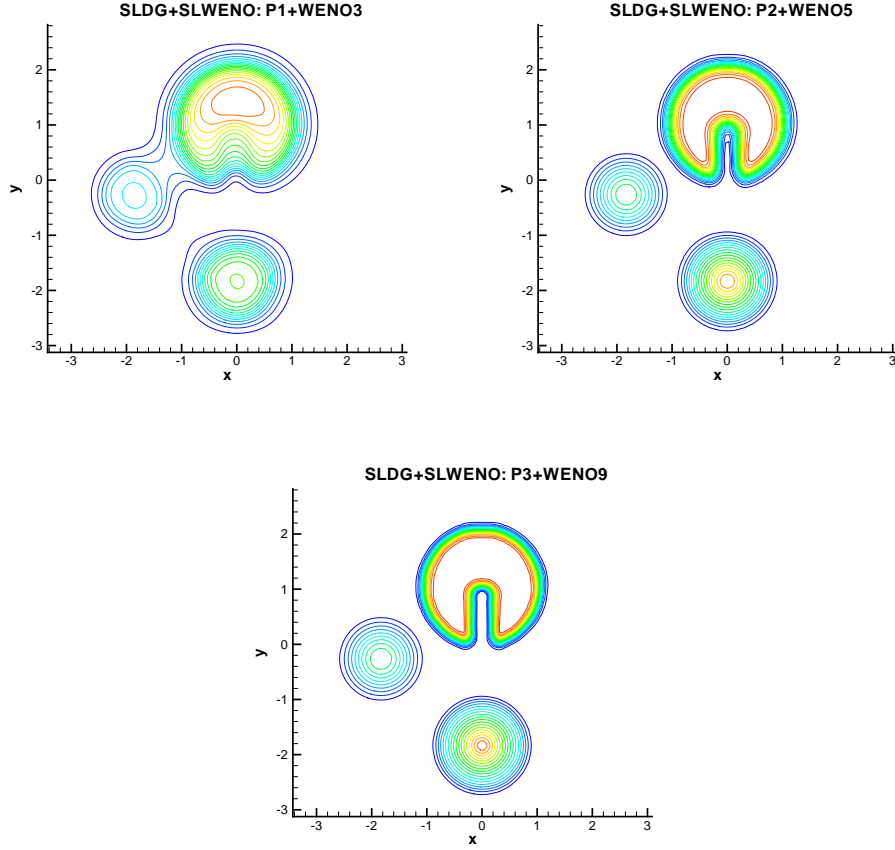


Figure 4.2: Rigid body rotation with the initial condition in Figure 4.1. Uniform meshes with $N_x \times N_y = 100 \times 100$. TVB constant $M=1.0$. $CFL = 2.2$. $T=12\pi$. Hybrid scheme: SL DG combined with SL WENO.

2. Energy:

$$\text{Energy} = \int_v \int_x f(x, v, t) v^2 dx dv + \int_x E^2(x, t) dx, \quad (4.5)$$

where $E(x, t)$ is the electric field.

3. Entropy:

$$\text{Entropy} = \int_v \int_x f(x, v, t) \log(f(x, v, t)) dx dv. \quad (4.6)$$

Tracking relative deviations of these quantities numerically will be a good measure of the quality of numerical schemes. The relative deviation is defined to be the deviation away from the corresponding initial value divided by the magnitude of the initial value. It is expected

that our scheme will conserve mass. However, the positivity of f will not be preserved. Thus, when numerically computing the entropy, we compute $\int_v \int_x f(x, v, t) |\log(f(x, v, t))| dx dv..$

Below, we first present the performance of the proposed hybrid scheme for two stream instability. In this example, we will demonstrate (1) the high order spatial accuracy and the second order temporal accuracy of the proposed scheme; (2) the performance of the proposed hybrid method in resolving solutions and in preserving theoretically conserved physical norms; (3) the robustness of finite difference WENO scheme for velocities compared with spectral method and pure SL DG scheme.

Example 4.3. Consider two stream instability [15], with an unstable initial distribution function:

$$f(x, v, t = 0) = \frac{2}{7\sqrt{2\pi}}(1 + 5v^2)(1 + \alpha((\cos(2kx) + \cos(3kx))/1.2 + \cos(kx))) \exp(-\frac{v^2}{2}) \quad (4.7)$$

with $\alpha = 0.01$, $k = 0.5$, the length of the domain in the x direction is $L = \frac{2\pi}{k}$ and the background ion distribution function is fixed, uniform and chosen so that the total net charge density for the system is zero.

Firstly, we want to test spatial and temporal accuracy of the hybrid methods. To minimize the error from truncating the domain in v -direction, we let $v_{max} = 2\pi$. We compute a reference numerical solution with very fine mesh. We remark that the overall numerical error is due to two parts: spatial and temporal error. To test spatial accuracy of DG in x -direction, we make the mesh in v -direction to be fine enough and time step to be sufficiently small, so that spatial error dominates. We report the L^2 error and the order of accuracy for two hybrid methods: SL DG combined with SL WENO in Table 4.7 and RK DG combined with SL WENO in Table 4.8. Expected $k + 1$ orders of spatial accuracy are observed. To test temporal accuracy, there is a lower bound in the time step size that we need to respect. When the time step is too small, spatial error becomes dominant. we let $\Delta t = \Delta x$ to test the temporal accuracy. In Table 4.9 we report the L^2 error and the

order of accuracy for two hybrid methods: SL/RK DG P^3 combined with SL WENO9 for second order Strang splitting. Expected second order temporal accuracy is observed. Note that the errors from two hybrid methods are comparable, due to the fact that splitting error dominates for a large time step.

Then we test the reliability of the hybrid methods after a long time integration with $v_{max} = 5$ and $\Delta t = \Delta x$. In Figure 4.3, we show the numerical results of hybrid methods at $T = 53$. The filamentation solution structures are well resolved by the hybrid method. Time evolution of discrete L^1 norm, L^2 norm, kinetic energy and entropy of hybrid methods with different orders are reported in Figure 4.4. As expected, the physical quantities, which are conserved in the continuous VP system, are better preserved by higher order hybrid method. In Figures 4.5 we show 3D plots of the distribution function f at different instances of time. Good resolutions can be observed without oscillations. Our results are comparable to those that have been reported by Filbet and Sonnendrücker in [15] where the performance of several numerical schemes are compared. Since DG method is used in x-direction, nonuniform mesh is allowed. Figure 4.6 presents the mesh and numerical solution of a hybrid method (RK DG scheme with P^3 in x-direction and SL WENO9 scheme in v-direction) at $T = 53$ using a non-uniform mesh which is 20% random perturbation of the uniform mesh in x-direction with $N_x \times N_v = 64 \times 160$. Due to the non-uniform distribution of the mesh, we use LDG scheme instead of FFT to solve the Poisson equation.

An alternative way of advection for the velocity acceleration/deceleration is the spectral method. The numerical results of the scheme using SL DG in x-direction and spectral method in v-direction are presented in Figure 4.7 at different times. When the structure of solution is simple (see the left panel in Figure 4.7), the spectral method performs well. However, as the numerical mesh no longer supports the filamentation solution structures that are developed over long time, serious spurious oscillations are observed (see the right panel of Figure 4.7).

Finally, we use this example to give a comparison between the method using in both

Table 4.7: Two stream instability. Hybrid method with SL DG and SL WENO. L^2 errors and numerical orders of accuracy on uniform meshes with $N_x \times N_y$ cells. $\Delta t = 0.005\Delta x$. $T=0.5$. The reference solution is computed with $N_x \times N_y = 192 \times 630$.

	$P^2 + WENO5$		$P^3 + WENO9$	
mesh	L^2 error	order	L^2 error	order
16×210	1.49E-04	–	1.05E-05	–
32×210	1.85E-05	3.01	6.55E-07	4.00
48×210	5.50E-06	3.00	1.29E-07	4.00
64×210	2.31E-06	3.02	4.17E-08	3.94

Table 4.8: Two stream instability. Hybrid method with RK DG and SL WENO. L^2 errors and numerical orders of accuracy on uniform meshes with $N_x \times N_y$ cells. $\Delta t = 0.005\Delta x$. $T=0.5$. The reference solution is computed with $N_x \times N_y = 192 \times 630$

	$P^2 + WENO5$		$P^3 + WENO9$	
mesh	L^2 error	order	L^2 error	order
16×210	1.54E-04	–	1.06E-05	–
32×210	1.92E-05	3.01	6.64E-07	4.00
48×210	5.69E-06	2.99	1.31E-07	4.00
64×210	2.39E-06	3.02	4.22E-08	3.94

spatial and velocity directions and the proposed hybrid methods. We set $N_x \times N_v = 64 \times 128$ for SL DG scheme (P^3 polynomial in both x- and v- directions) and $N_x \times N_v = 64 \times 512$ for hybrid method (SL DG scheme with P^3 in x-direction and SL WENO9 scheme in v-direction) for a comparable resolution. Figure 4.8 gives 3D plots of the numerical solution in the region where filamentation structures are developed. Milder numerical sawtooth-shaped oscillations are observed for hybrid method than that for pure SL DG schemes, when the numerical solution is under-resolved.

Example 4.4. Consider weak Landau damping for the Vlasov-Poisson system with initial condition:

$$f(x, v, t = 0) = \frac{1}{\sqrt{2\pi}}(1 + \alpha \cos(kx)) \exp\left(-\frac{v^2}{2}\right), \quad (4.8)$$

Table 4.9: Two stream instability. Hybrid methods with SL/RK DG P^3 and SL WENO9. L^2 errors and numerical orders of accuracy on uniform meshes with $N_x \times N_y$ cells. The reference is computed with $N_x \times N_v = 630 \times 630, \Delta t = \Delta x, T=1$.

	SL DG P^3 +SL WENO9		RK DG P^3 +SL WENO9	
mesh	L^2 error	order	L^2 error	order
70×70	3.23E-04	–	3.23E-04	–
90×90	1.93E-04	2.05	1.93E-04	2.05
126×126	9.59E-05	2.08	9.59E-05	2.08
210×210	3.20E-05	2.15	3.20E-05	2.15

where $\alpha = 0.01$. When the perturbation parameter $\alpha = 0.01$ is small enough, the VP system can be approximated by linearization around the Maxwellian equilibrium $f^0(v) = \frac{1}{\sqrt{2\pi}} e^{-\frac{v^2}{2}}$. The analytical damping rate of electric field can be derived accordingly [17]. We test our scheme with different k 's and compare the numerical damping rates with theoretical values. In the simulations, we set $N_x = 64, N_v = 160, v_{max} = 5$ and $\Delta t = \Delta x$. We plot the evolution of electric field in L^2 norm in Figure 4.9 for $k = 0.5, k = 0.4$ and $k = 0.3$. The correct decay rates of the electric field are observed, benchmarked with all the theoretical values (solid black lines in the figure). The time evolution of discrete L^1 norm, L^2 norm, kinetic energy and entropy of hybrid methods with different orders are reported in Figure 4.10. In order to save spaces, we only report the result when $k = 0.5$. In this case, the total mass is observed to be exactly conserved. Other physical quantities are well preserved.

Example 4.5. Consider strong Landau damping. The initial condition is equation (4.8), with $\alpha = 0.5$ and $k = 0.5$. In Figure 4.11, the evolution of L^2 norms of electric field is provided. The linear decay rate of different orders of hybrid methods are all approximately $\gamma_1 = -0.2812$, which is identical to the value computed by Cheng and Knorr [6]. It is a little smaller than the value of -0.292 reported by Rossmannith and Seal in [37] and -0.287 reported by Heath et. al in [21]. We also compute the growth rates of hybrid methods, which are approximately $\gamma_2 = 0.0813$ of SL DG P^3 combined with SL WENO9, $\gamma_2 = 0.0778$

of SL DG P^2 combined with SL WENO5 and $\gamma_2 = 0.0770$ of SL DG P^1 combined with SL WENO3. They are all consistent with the value of 0.0815 computed by Rossmannith and Seal in [37] and 0.0746 by Heath et. al in [21]. Numerical solutions of the hybrid methods with different orders at $T=30$ are plotted in Figure 4.12. Better resolutions are observed with higher order method. Figure 4.13 gives the numerical solution of strong Landau damping at different times using hybrid method of SL DG P^3 combined with SL WENO9, the results are comparable to what are shown in [33]. The time evolution of discrete L^1 norm, L^2 norm, kinetic energy and entropy of hybrid methods with different orders are reported in Figure 4.14. It is clear that high order hybrid methods better preserve physical quantities than low order methods, as expected. We remark that because the proposed hybrid methods are not positivity preserving, L^1 norms of numerical solutions are not exactly preserved, although the methods are mass conservative.

Example 4.6. Consider the symmetric two stream instability [13], with the initial condition

$$f(x, v, t = 0) = \frac{1}{2v_{th}\sqrt{2\pi}} \left[\exp\left(-\frac{(v-u)^2}{2v_{th}^2}\right) + \exp\left(-\frac{(v+u)^2}{2v_{th}^2}\right) \right] (1 + \alpha \cos(kx)). \quad (4.9)$$

The background ion distribution function is fixed, uniform and chosen so that the total net charge density for the system is zero. We first let $\alpha = 0.001$, $u = 2.4$, $v_{th} = 1$ and $k = 0.2$. The linear growth rate of electric field after some time is 0.2258, which can be derived by the same procedure as Landau damping. In Figure 4.15, we plot the evolution of electric field in L^2 norm. The correct growth rates of the electric field are observed, benchmarked with the theoretical value. We then let $\alpha = 0.05$, $u = 0.99$, $v_{th} = 0.3$ and $k = \frac{2}{13}$. This case is studied in [35, 36] by SL WENO and SL DG scheme, respectively. In Figures 4.16, we report the numerical results approximating the distribution solution f . Time evolution of discrete L^1 norm, L^2 norm, kinetic energy and entropy of hybrid methods with different orders are reported in Figure 4.17. Again, the high order methods in general do a better job in resolving filamentation structures and preserving the physical quantities than low order

ones. Finally, we remark that with strong perturbation, nonlinear effect of higher modes becomes dominant. The evolution of electric field does not agree with theoretical value in linear analysis. Thus we omit to present the evolution of electric field in this paper.

5 Concluding remarks

In this paper, a family of hybrid SL numerical methods are designed to solve the VP system. The proposed hybrid methods combine SL/Eulerian RK DG scheme and SL finite difference WENO scheme for the spacial advection and velocity acceleration/deceleration, respectively. In the SL framework, there is no time step restriction for the linear stability, so the allowance of large time step can greatly save computational cost. DG scheme is adopted for spacial advection due to its compactness. RK DG offers the flexibility to deal with complicated geometries and boundary conditions when high dimensional problems are considered. SL WENO scheme is adopted for velocity advection due to its robustness to resolve filamentation solution structures in the VP system. A WENO limiting strategy is used to control artificial oscillations produced by DG scheme. We apply the hybrid methods to several test examples, such as linear advection, rigid body rotation and the VP system to demonstrate the performance. Improving the second order accuracy in time and extending the hybrid methods to high dimensional Vlasov-Poisson and Vlasov-Maxwell systems constitute our future work.

References

- [1] D. BARNES, T. KAMIMURA, J. LEBOEUF, AND T. TAJIMA, *Implicit particle simulation of magnetized plasmas*, Journal of Computational Physics, 52 (1983), pp. 480–502.
- [2] M. BEGUE, A. GHIZZO, P. BERTRAND, E. SONNENDRUCKER, AND O. COULAUD, *Two-dimensional semi-Lagrangian Vlasov simulations of laser–plasma interaction in the relativistic regime*, Journal of Plasma Physics, 62 (1999), pp. 367–388.
- [3] N. BESSE AND E. SONNENDRUCKER, *Semi-Lagrangian schemes for the Vlasov equation on an unstructured mesh of phase space*, Journal of Computational Physics, 191 (2003), pp. 341–376.
- [4] J. BORIS AND D. BOOK, *Flux-corrected transport. I. SHASTA, A fluid transport algorithm that works*, Journal of computational physics, 11 (1973), pp. 38–69.
- [5] J. CARRILLO AND F. VECIL, *Nonoscillatory interpolation methods applied to Vlasov-based models*, SIAM Journal on Scientific Computing, 29 (2007), p. 1179.
- [6] C. CHENG AND G. KNORR, *The integration of the Vlasov equation in configuration space*, Journal of Computational Physics, 22 (1976), pp. 330–351.
- [7] Y. CHENG, I. GAMBA, AND J. PROFT, *Positivity-preserving discontinuous Galerkin schemes for linear Vlasov-Boltzmann transport equations*, Mathematics of Computation, (to appear).
- [8] B. COCKBURN, S. HOU, AND C.-W. SHU, *The Runge-Kutta local projection discontinuous Galerkin finite element method for conservation laws IV: the multidimensional case*, Mathematics of Computation, 54 (1990), pp. 545–581.

- [9] B. COCKBURN, C. JOHNSON, C.-W. SHU, AND E. TADMOR, *Advanced numerical approximation of nonlinear hyperbolic equations*, Springer New York, 1998.
- [10] B. COCKBURN, S. LIN, AND C.-W. SHU, *TVB Runge-Kutta local projection discontinuous Galerkin finite element method for conservation laws III: one-dimensional systems*, Journal of Computational Physics, 84 (1989), pp. 90–113.
- [11] B. COCKBURN AND C.-W. SHU, *TVB Runge-Kutta local projection discontinuous Galerkin finite element method for conservation laws II: general framework*, Mathematics of Computation, (1989), pp. 411–435.
- [12] ———, *The Runge-Kutta discontinuous Galerkin method for conservation laws V: multi-dimensional systems*, Journal of Computational Physics, 141 (1998), pp. 199–224.
- [13] N. CROUSEILLES, M. MEHRENBARGER, AND E. SONNENDRUCKER, *Conservative semi-Lagrangian schemes for Vlasov equations*, Journal of Computational Physics, 229 (2010), pp. 1927–1953.
- [14] E. FIJALKOW, *A numerical solution to the vlasov equation*, Computer physics communications, 116 (1999), pp. 319–328.
- [15] F. FILBET AND E. SONNENDRUCKER, *Comparison of Eulerian Vlasov solvers*, Computer Physics Communications, 150 (2003), pp. 247–266.
- [16] F. FILBET, E. SONNENDRUCKER, AND P. BERTRAND, *Conservative numerical schemes for the Vlasov equation*, Journal of Computational Physics, 172 (2001), pp. 166–187.
- [17] B. FRIED AND S. CONTE, *The plasma dispersion function*, The Plasma Dispersion Function, New York: Academic Press, 1961, 1 (1961).

- [18] A. FRIEDMAN, A. LANGDON, AND B. COHEN, *A direct method for implicit particle-in-cell simulation*, Comments Plasma Phys. Controlled Fusion, 6 (1981), pp. 225–236.
- [19] A. FRIEDMAN, S. PARKER, S. RAY, AND C. BIRDSALL, *Multi-scale particle-in-cell plasma simulation*, Journal of Computational Physics, 96 (1991), pp. 54–70.
- [20] S. GOTTLIEB, D. KETCHESON, AND C.-W. SHU, *High order strong stability preserving time discretizations*, Journal of Scientific Computing, 38 (2009), pp. 251–289.
- [21] R. HEATH, I. GAMBA, P. MORRISON, AND C. MICHLER, *A discontinuous Galerkin method for the Vlasov-Poisson system*, Journal of Computational Physics, (2011).
- [22] J. HEIKKINEN, S. JANHUNEN, T. KIVINIEMI, AND F. OGANDO, *Full f gyrokinetic method for particle simulation of tokamak transport*, Journal of Computational Physics, 227 (2008), pp. 5582–5609.
- [23] C. HU AND C.-W. SHU, *Weighted essentially non-oscillatory schemes on triangular meshes*, Journal of Computational Physics, 150 (1999), pp. 97–127.
- [24] F. HUOT, A. GHIZZO, P. BERTRAND, E. SONNENDRUCKER, AND O. COULAUD, *Instability of the time splitting scheme for the one-dimensional and relativistic Vlasov–Maxwell system*, Journal of Computational Physics, 185 (2003), pp. 512–531.
- [25] G. JACOBS AND J. HESTHAVEN, *Implicit-explicit time integration of a high-order particle-in-cell method with hyperbolic divergence cleaning*, Computer Physics Communications, 180 (2009), pp. 1760–1767.
- [26] G. JIANG AND C.-W. SHU, *Efficient implementation of weighted ENO schemes*, Journal of Computational Physics, 126 (1996), pp. 202–228.
- [27] A. LANGDON, B. COHEN, AND A. FRIEDMAN, *Direct implicit large time-step particle simulation of plasmas*, Journal of Computational Physics, 51 (1983), pp. 107–138.

- [28] R. LEVEQUE, *High-resolution conservative algorithms for advection in incompressible flow*, SIAM Journal on Numerical Analysis, (1996), pp. 627–665.
- [29] X. LIU, S. OSHER, AND T. CHAN, *Weighted essentially non-oscillatory schemes*, Journal of Computational Physics, 115 (1994), pp. 200–212.
- [30] T. NAKAMURA AND T. YABE, *Cubic interpolated propagation scheme for solving the hyper-dimensional vlasovpoisson equation in phase space*, Computer Physics Communications, 120 (1999), pp. 122–154.
- [31] F. PARRA AND P. CATTO, *Comment on "On higher order corrections to gyrokinetic Vlasov–Poisson equations in the long wavelength limit"* [*Phys. Plasmas* [bold 16], 044506 (2009)], Physics of Plasmas, 16 (2009), p. 124701.
- [32] J. QIU AND C.-W. SHU, *Runge-Kutta discontinuous Galerkin method using WENO limiters*, SIAM Journal on Scientific Computing, 26 (2005), pp. 907–929.
- [33] J.-M. QIU AND A. CHRISTLIEB, *A Conservative high order semi-Lagrangian WENO method for the Vlasov Equation*, Journal of Computational Physics, 229 (2010), pp. 1130–1149.
- [34] J.-M. QIU AND C.-W. SHU, *Conservative high order semi-Lagrangian finite difference WENO methods for advection in incompressible flow*, Journal of Computational Physics, 230 (2011), pp. 863–889.
- [35] —, *Conservative semi-Lagrangian finite difference WENO formulations with applications to the Vlasov equation*, Communications in Computational Physics, 10 (2011), pp. 979–1000.
- [36] —, *Positivity preserving semi-Lagrangian discontinuous Galerkin methods for Vlasov simulations*, Journal of Computational Physics, (to appear).

- [37] J. ROSSMANITH AND D. SEAL, *A positivity-preserving high-order semi-Lagrangian discontinuous Galerkin scheme for the Vlasov-Poisson equations*, Journal of Computational Physics, 230 (2011), pp. 6203–6232.
- [38] E. SONNENDRUCKER, J. ROCHE, P. BERTRAND, AND A. GHIZZO, *The semi-Lagrangian method for the numerical resolution of the Vlasov equation*, Journal of Computational Physics, 149 (1999), pp. 201–220.
- [39] T. UMEDA, M. ASHOUR-ABDALLA, AND D. SCHRIVER, *Comparison of numerical interpolation schemes for one-dimensional electrostatic Vlasov code*, Journal of Plasma Physics, 72 (2006), pp. 1057–1060.
- [40] V. VAHEDI, G. DiPESO, C. BIRDSALL, M. LIEBERMAN, AND T. ROGNLIEN, *Capacitive RF discharges modelled by particle-in-cell Monte Carlo simulation. I. Analysis of numerical techniques*, Plasma Sources Science and Technology, 2 (1993), p. 261.
- [41] Z. XIONG, R. COHEN, T. ROGNLIEN, AND X. XU, *A high-order finite-volume algorithm for Fokker-Planck collisions in magnetized plasmas*, Journal of Computational Physics, 227 (2008), pp. 7192–7205.
- [42] X. XU, K. BODI, R. COHEN, S. KRASHENINNIKOV, AND T. ROGNLIEN, *TEMPEST simulations of the plasma transport in a single-null tokamak geometry*, Nuclear Fusion, 50 (2010), p. 064003.
- [43] X. XU, Z. XIONG, M. DORR, J. HITTINGER, K. BODI, J. CANDY, B. COHEN, R. COHEN, P. COLELLA, G. KERBEL, ET AL., *Edge gyrokinetic theory and continuum simulations*, Nuclear fusion, 47 (2007), p. 809.
- [44] X. ZHANG AND C. SHU, *On maximum-principle-satisfying high order schemes for scalar conservation laws*, Journal of Computational Physics, 229 (2010), pp. 3091–3120.

- [45] T. ZHOU, Y. GUO, AND C.-W. SHU, *Numerical study on Landau damping*, *Physica D: Nonlinear Phenomena*, 157 (2001), pp. 322–333.
- [46] J. ZHU, J. QIU, C.-W. SHU, AND M. DUMBSER, *Runge-Kutta discontinuous Galerkin method using WENO limiters II: unstructured meshes*, *Journal of Computational Physics*, 227 (2008), pp. 4330–4353.

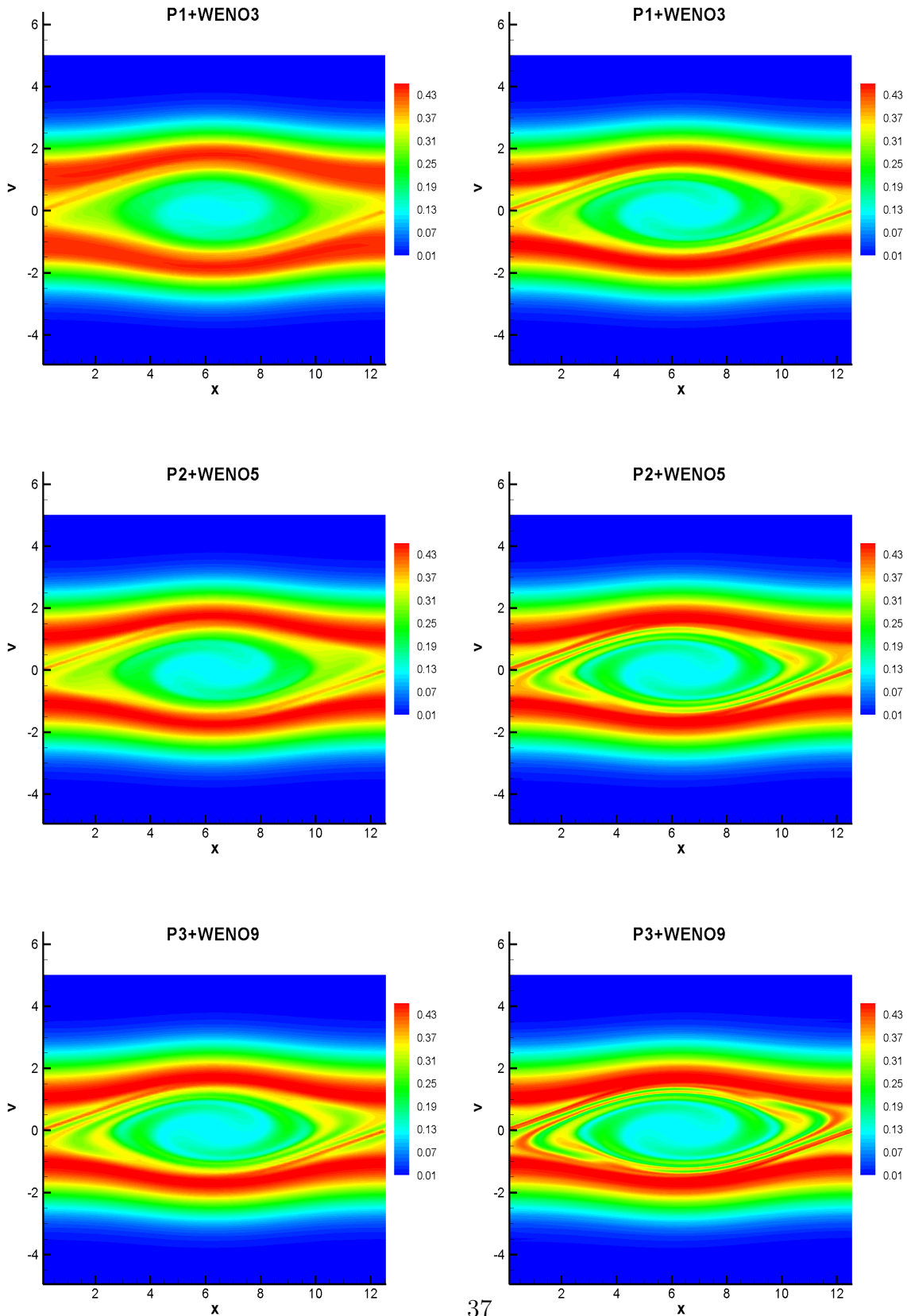


Figure 4.3: Two stream instability. TVB constant $M=1.0$. $T=53$. Hybrid scheme: SL DG combined with SL WENO. $N_x \times N_v = 64 \times 160$ (left), $N_x \times N_v = 128 \times 320$ (right).

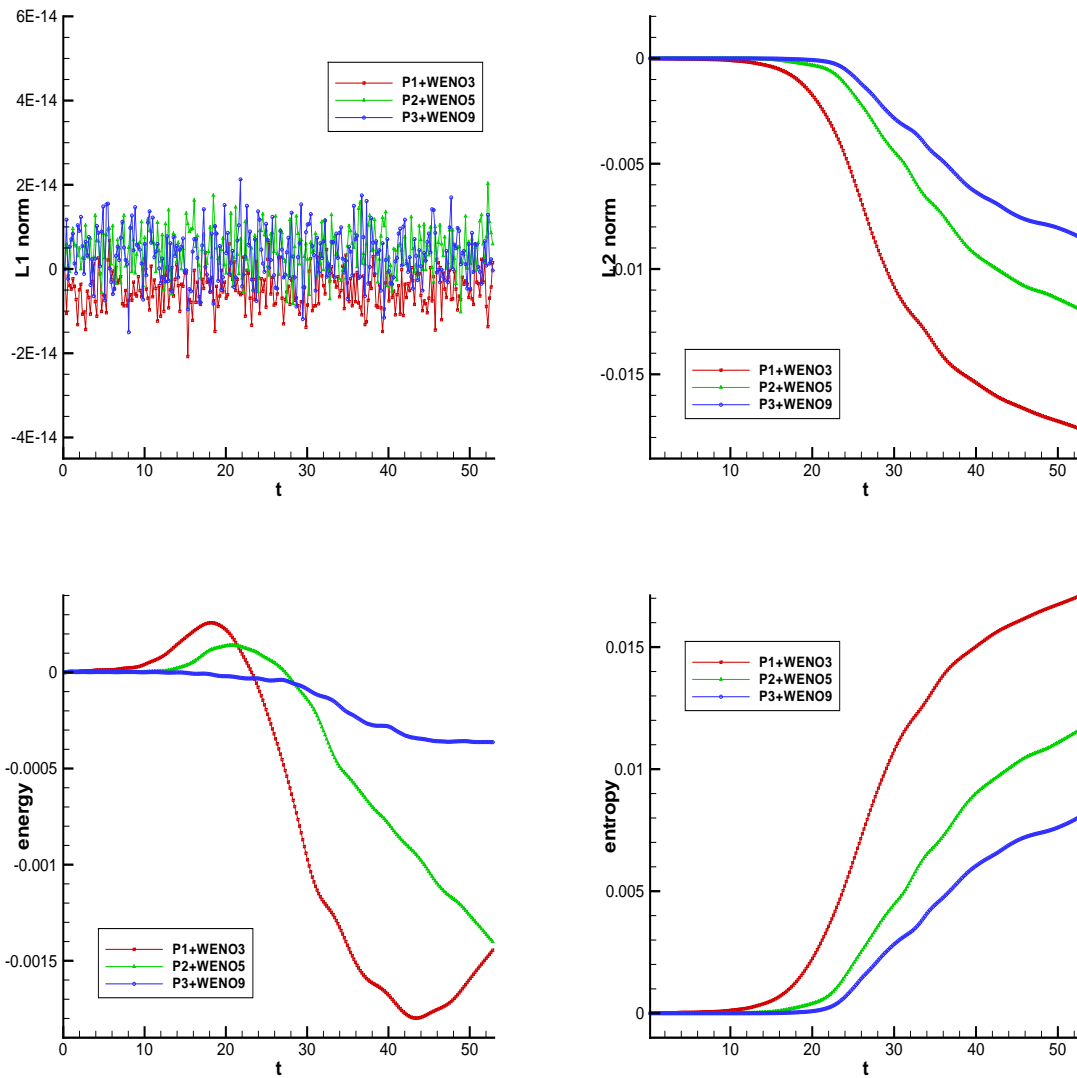


Figure 4.4: Two stream instability. Time evolution of the relative deviations of discrete L^1 norms (upper left), L^2 norms (upper right), kinetic energy norms (lower left) and entropy (lower right). TVB constant $M= 1.0$. Hybrid scheme: RK DG combined with SL WENO.

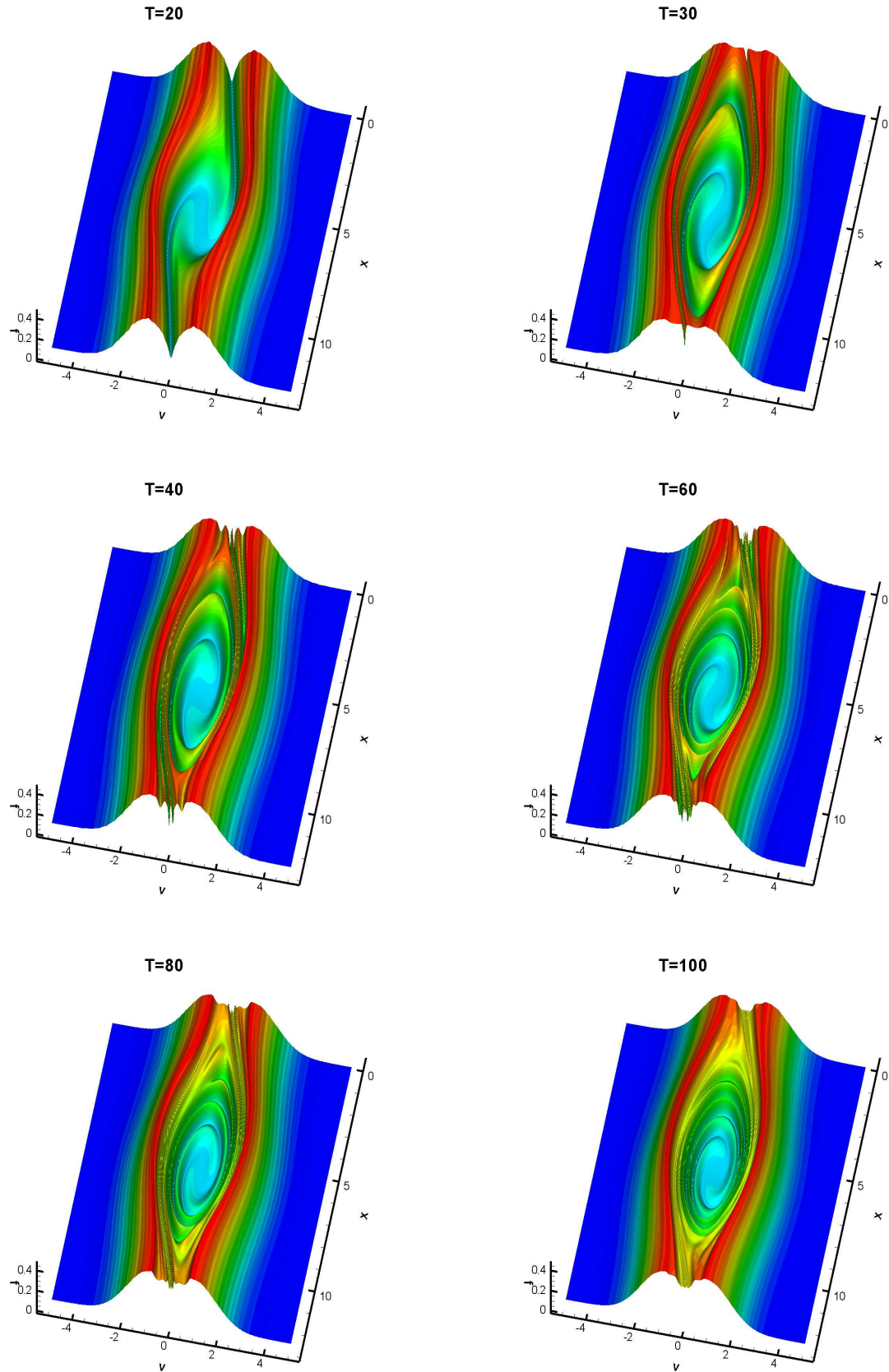


Figure 4.5: Two stream instability. TVB constant $M=1.0$. $N_x \times N_v = 128 \times 320$. 3D contour plot of distribution function. $T=20, 30, 40, 60, 80, 100$.

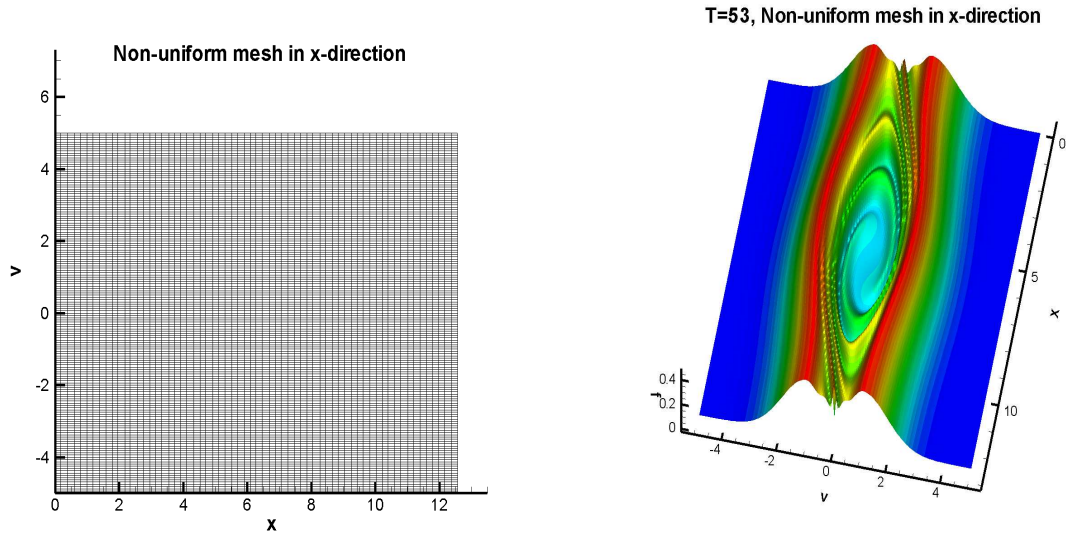


Figure 4.6: Two stream instability. Non-uniform mesh with 20% random perturbation of the uniform mesh $N_x \times N_v = 64 \times 160$. $T = 53$. Hybrid scheme: RK DG P^3 combined with SL WENO9.

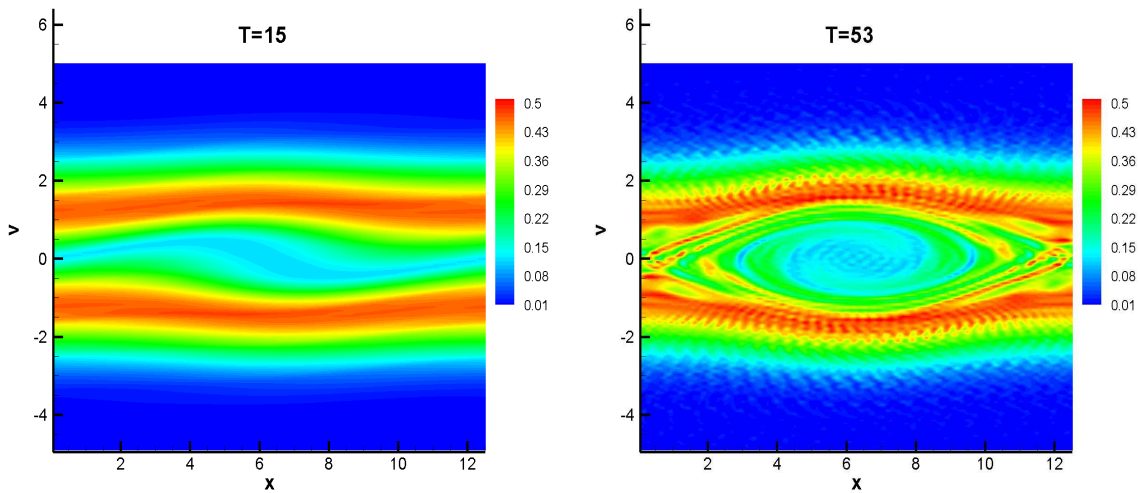


Figure 4.7: Two stream instability. Spectral method is adopted for velocity acceleration/deceleration. When $T = 15$, the structure of solution is simple, the performance of spectral method is good (left); when $T = 53$, the filamentation structures are generated, serious oscillations appear (right).

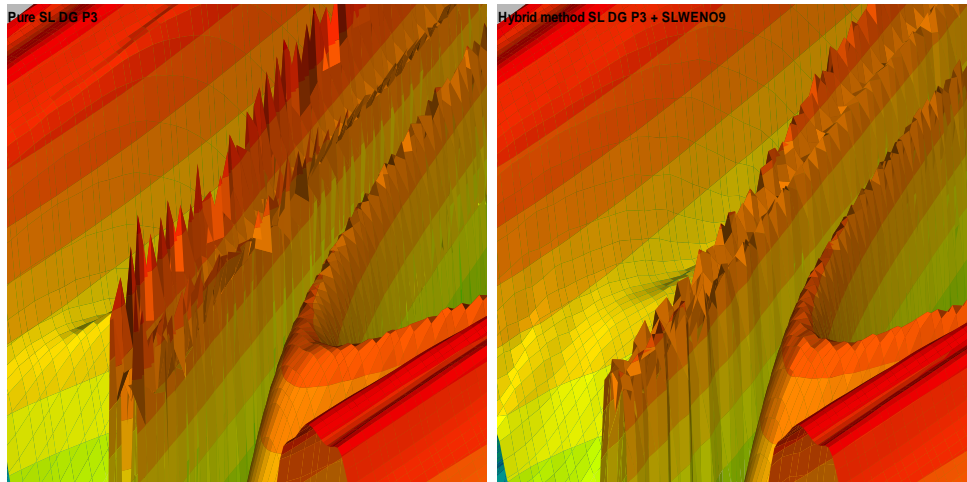


Figure 4.8: Two stream instability. Comparison between the SL DG scheme and hybrid methods. $T = 53$. Pure SL DG P^3 (left), hybrid method combined SL DG P^3 and SL WENO9 (right). Zoomed-in region to show more details. Much less artificial oscillations are observed of hybrid method.

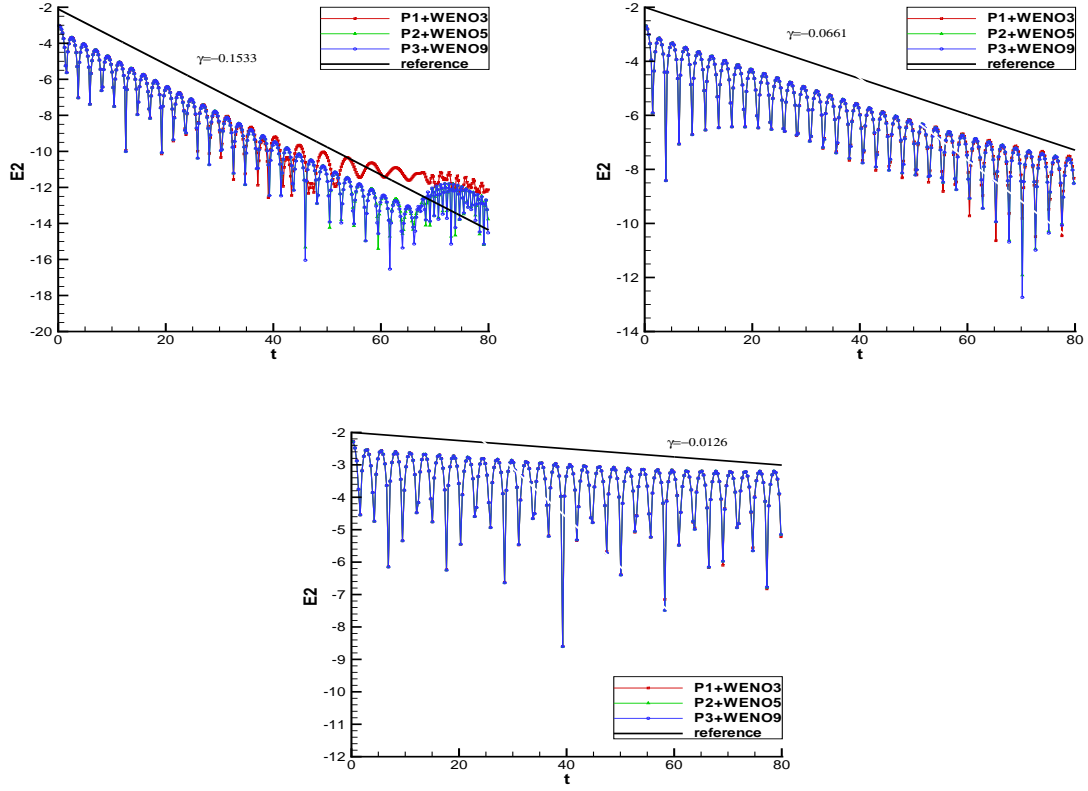


Figure 4.9: Weak Landau damping. Time evolution of electric field in L^2 norm. $k = 0.5$ (upper left), $k = 0.4$ (upper right) and $k = 0.3$ (lower)

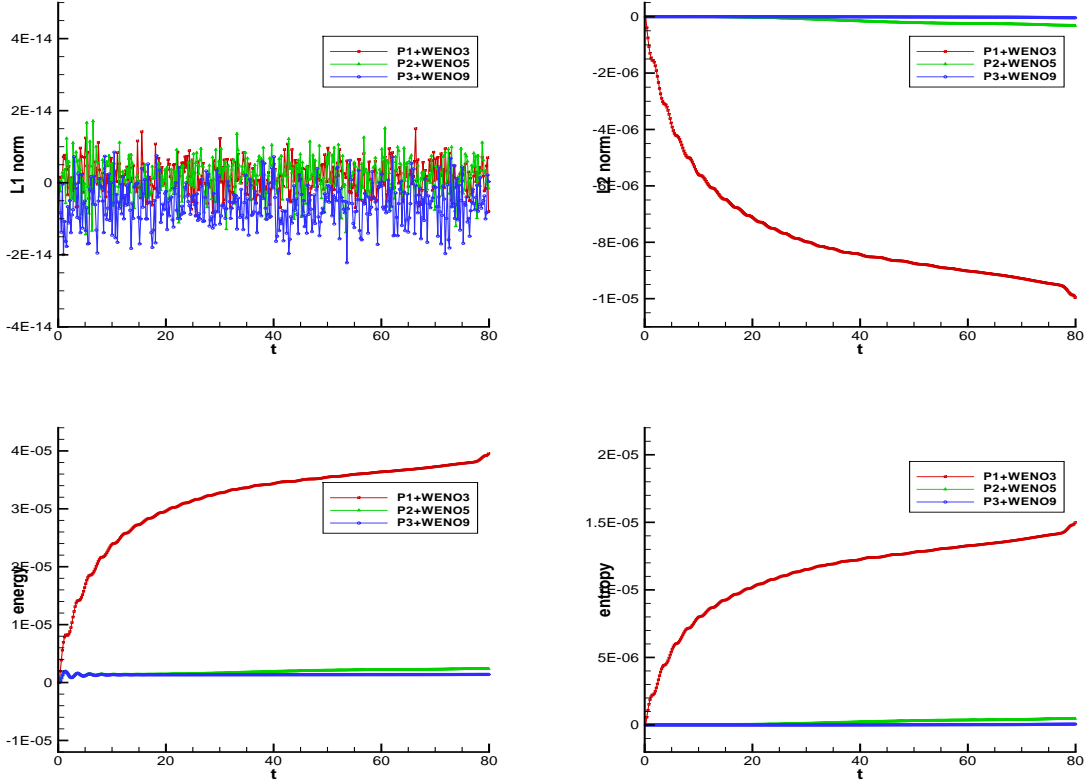


Figure 4.10: Weak Landau damping. Time evolution of the relative deviations of discrete L^1 norms (upper left), L^2 norms, kinetic energy norms (lower left) and entropy (lower right). TVB constant $M= 1.0$. Hybrid scheme: SL DG combined with SL WENO.

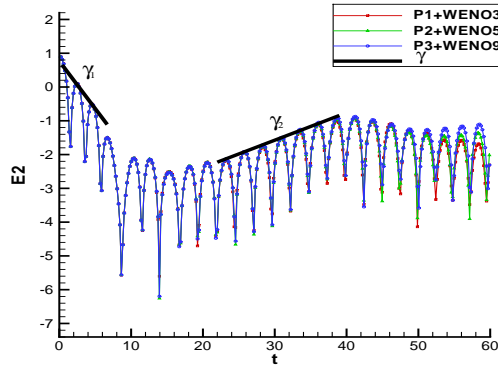


Figure 4.11: Strong Landau damping. Time evolution of electric field in L^2 norm.

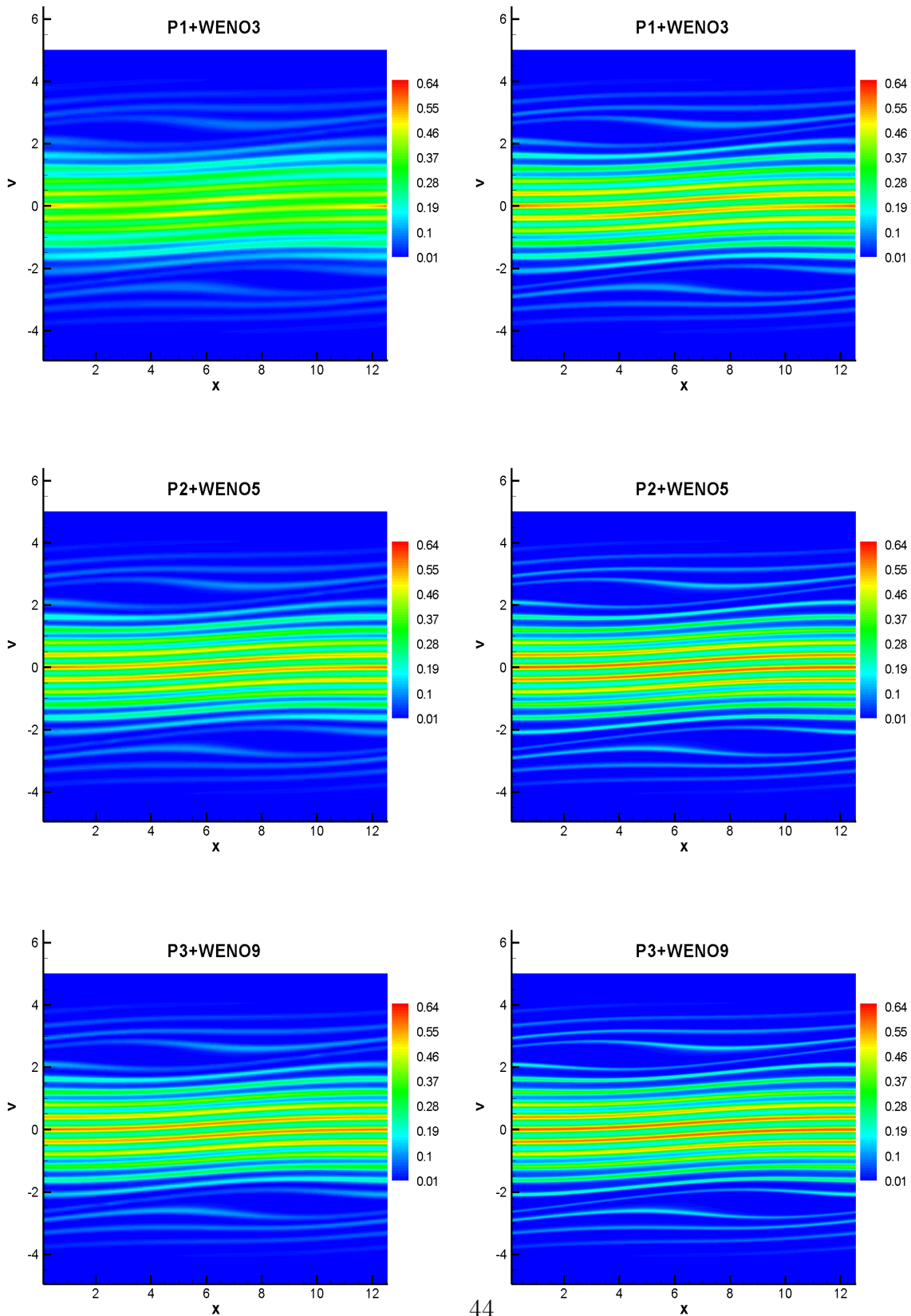


Figure 4.12: Strong Landau damping. TVB constant $M=1.0$. $T=30$. Hybrid scheme: SL DG combined with SL WENO. $N_x \times N_v = 64 \times 160$ (left), $N_x \times N_v = 128 \times 320$ (right).

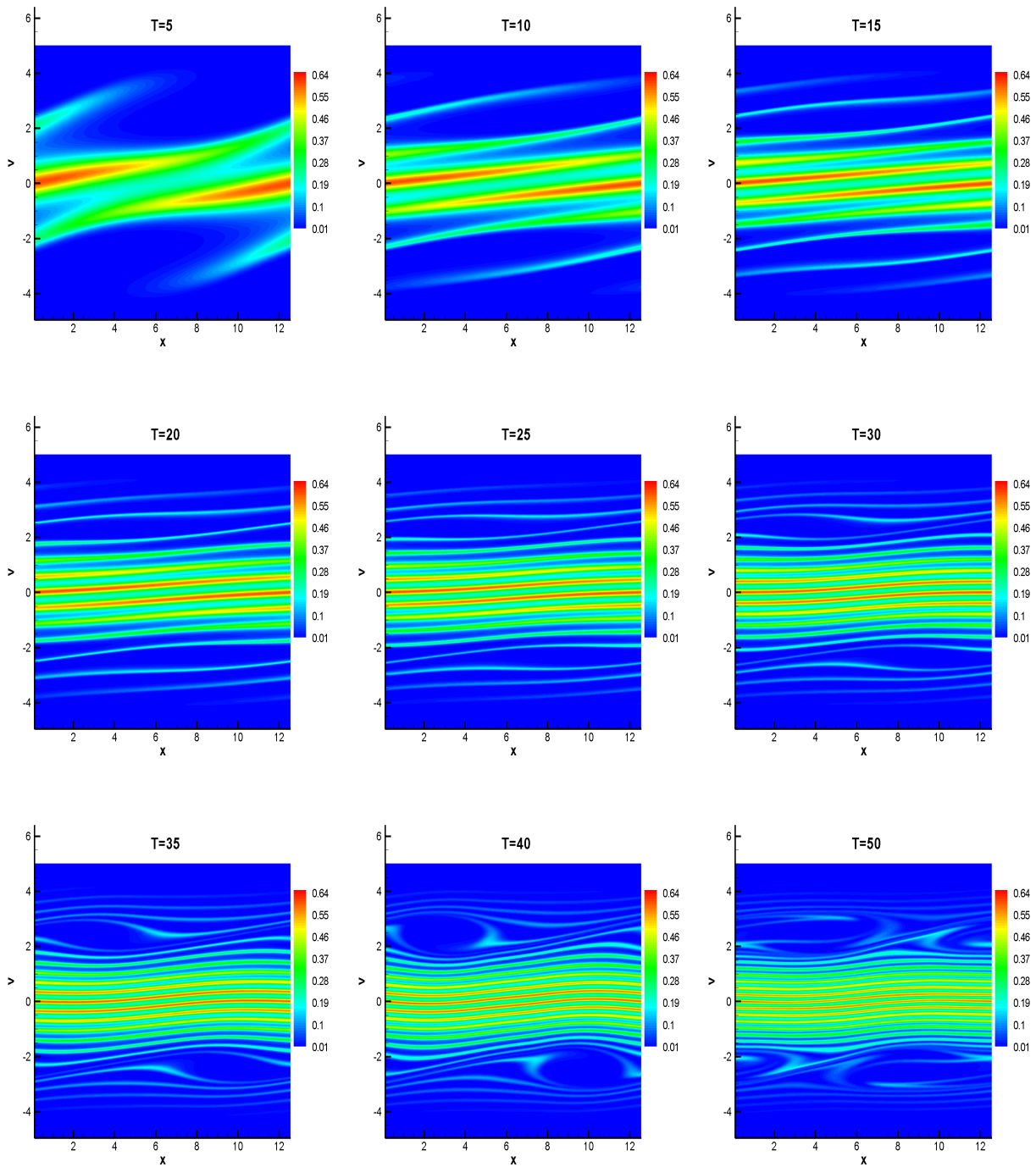


Figure 4.13: Strong Landau damping. TVB constant $M=1.0$. Time evolution of numerical solution at $T=5, 10, 15, 20, 25, 30, 35, 40, 50$. Hybrid scheme of SL DG P^3 combined with SLWENO9. $N_x \times N_y = 128 \times 320$.

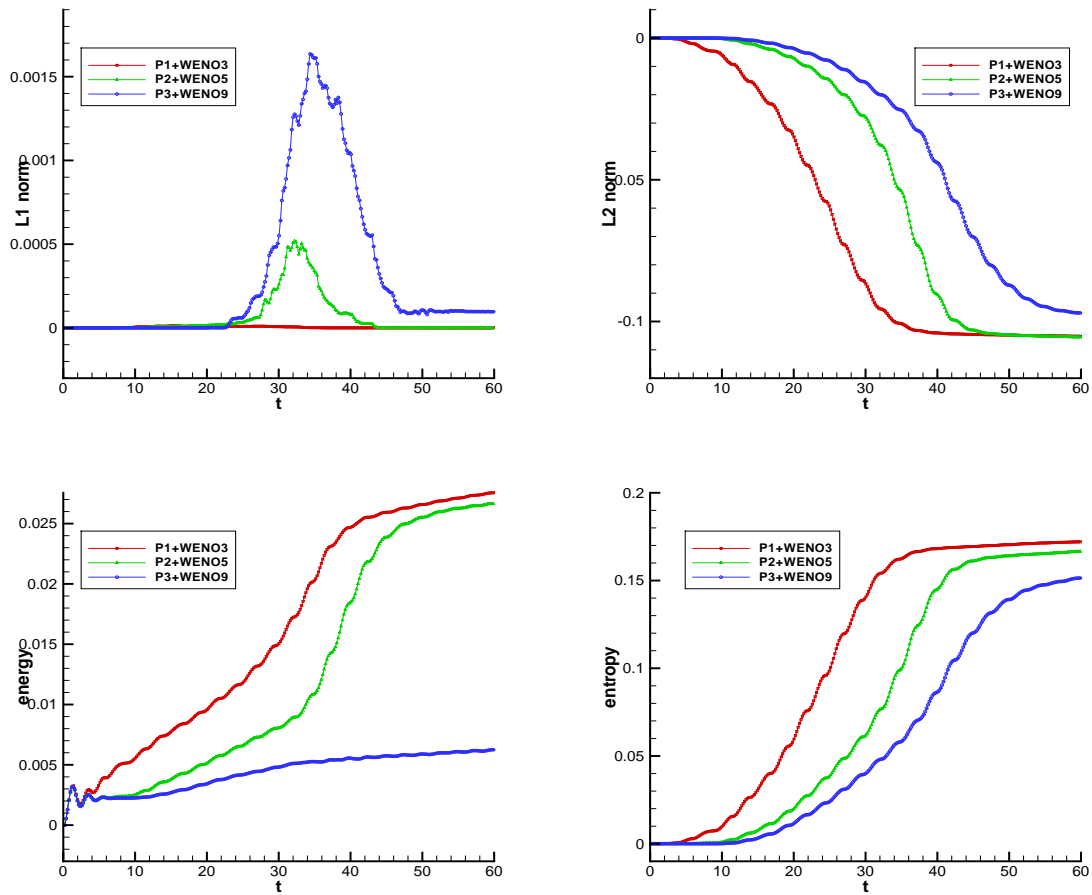


Figure 4.14: Strong Landau damping. Time evolution of the relative deviations of discrete L^1 norms (upper left), L^2 norms, kinetic energy norms (lower left) and entropy (lower right). TVB constant $M= 1.0$. Hybrid scheme: SL DG combined with SL WENO.

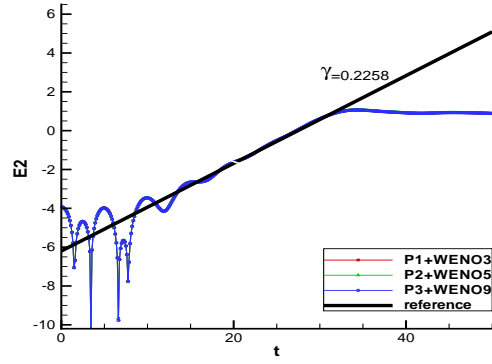


Figure 4.15: Two stream instability. Time evolution of electric field in L^2 norm. $\alpha = 0.001$, $u = 2.4$, $v_{th} = 1$ and $k = 0.2$.

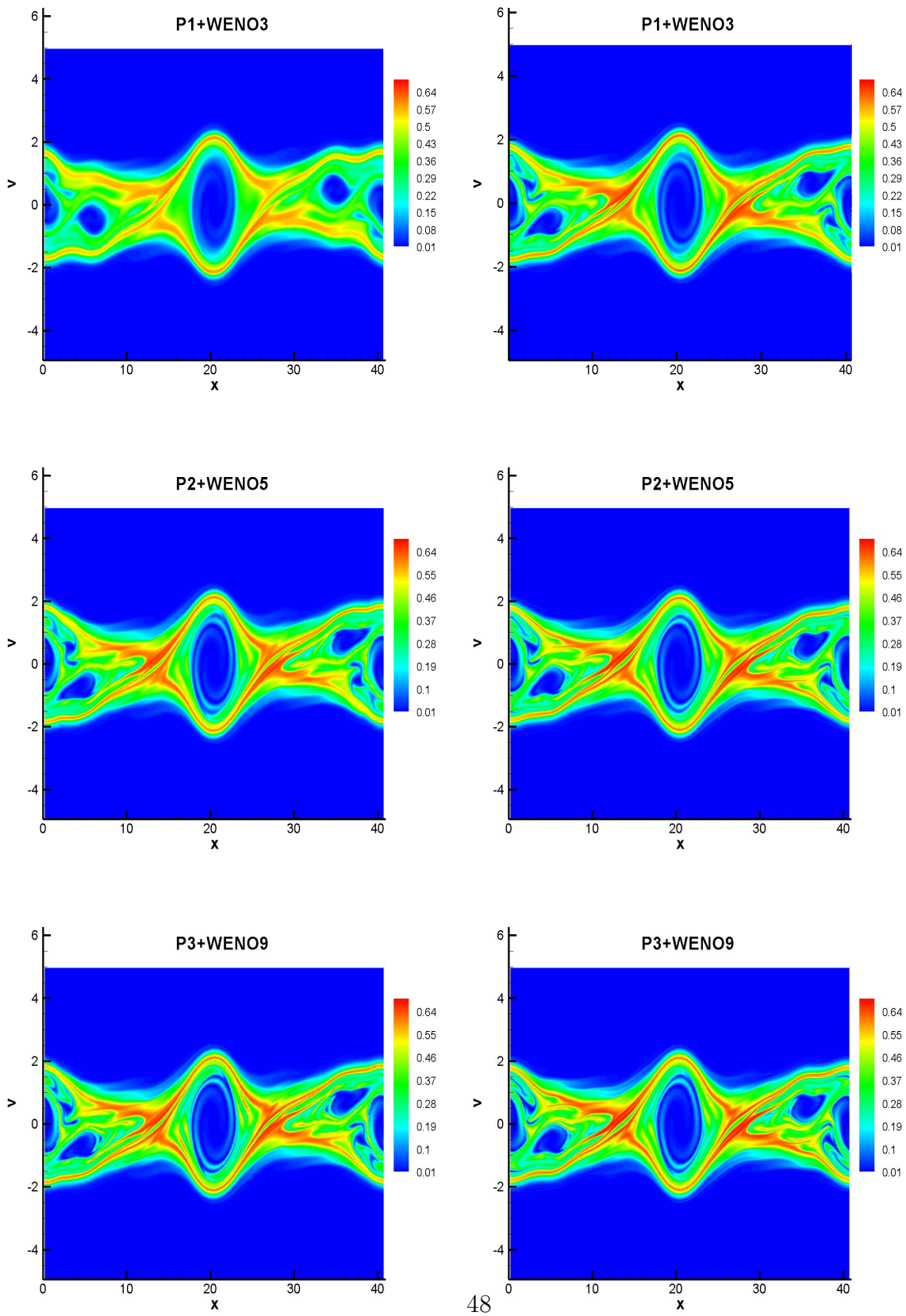


Figure 4.16: Two stream instability. TVB constant $M=3.0$. $T=70$. Hybrid scheme: SL DG combined with SL WENO. $N_x \times N_v = 128 \times 320$ (left), $N_x \times N_v = 256 \times 640$ (right).

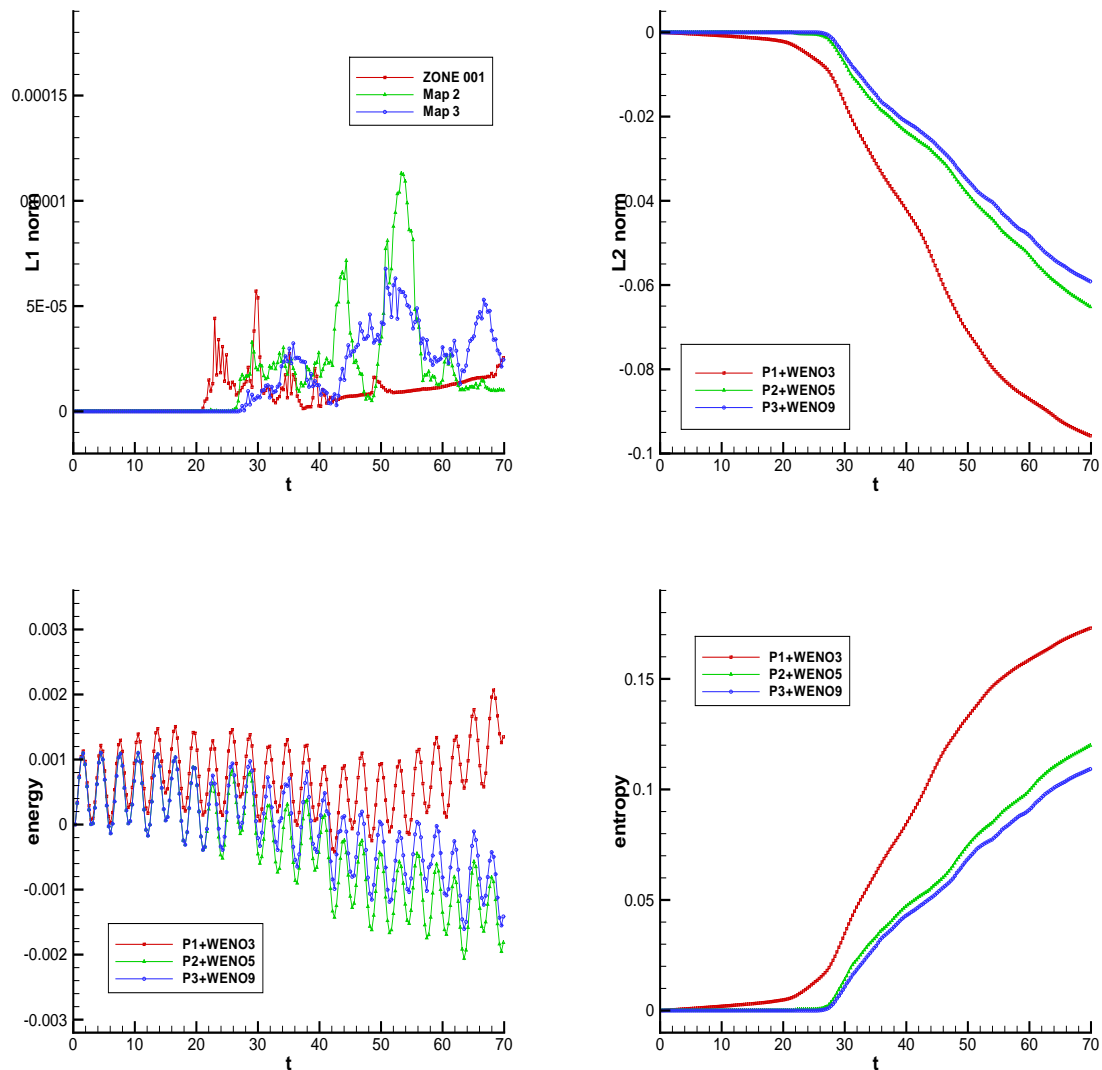


Figure 4.17: Two stream instability. Time evolution of the relative deviations of discrete L^1 norms (upper left), L^2 norms, kinetic energy norms (lower left) and entropy (lower right). TVB constant $M= 3.0$. Hybrid scheme: SL DG combined with SL WENO.